CHARACTERIZATION AND VALIDATION OF THE GP-3 EXPERIMENTAL RADAR SYSTEM

THESIS

Benjamin L. Crossley, Second Lieutenant, USAF

AFIT/GE/ENG/01M-06

DEPARTMENT OF THE AIR FORCE
AIR UNIVERSITY

AIR FORCE INSTITUTE OF TECHNOLOGY

Wright-Patterson Air Force Base, Ohio

The views expressed in this thesis are those of the author and do not reflect the official policy or position of the United States Air Force, Department of Defense, or the U. S. Government.

AFIT/GE/ENG/01M-06

CHARACTERIZATION AND VALIDATION OF THE GP-3 EXPERIMENTAL RADAR SYSTEM

THESIS

Presented to the Faculty

Department of Electrical and Computer Engineering

Graduate School of Engineering and Management

Air Force Institute of Technology

Air University

Air Education and Training Command

In Partial Fulfillment of the Requirements for the

Degree of Master of Science in Electrical Engineering

Benjamin L. Crossley, B.S.E.E.,

Second Lieutenant, USAF

March 2001

AFIT/GE/ENG/01M-06

CHARACTERIZATION AND VALIDATION OF THE GP-3 EXPERIMENTAL RADAR SYSTEM

Benjamin L. Crossley, B.S.E.E.
Second Lieutenant, USAF

Approved:

Dr. Michael A. Temple (Chairman)	5 Mar 01 Date
Maj Richard A. Raines	5 Mar 01 Date
Dr. Vittal P. Pyati	5 Mar. 01 Date

Acknowledgements

Having completed this endeavor, I would like to thank those who have supported me over the past year. I would first like to thank my thesis advisor, Dr. Mike Temple for his guidance and help. I am grateful to Ed Culpepper for providing everything I needed and being willing to help with any problems I encountered. I would also like to thank my committee members Major Richard Raines and Dr. Vittal Pyati. Most of all I would like to thank [redacted] for tolerating and feeding me and especially for motivating me to work. Thank you.

Benjamin Lee Crossley

Table of Contents

Table of Figures

Table of Tables

Abstract

The experimental GP-3 radar system was originally designed and built under contract for the Air Force Research Laboratory (AFRL). AFRL sought AFIT's support in characterizing the 'as delivered' performance of the GP-3. This research effort focused exclusively on software modifications and hardware validations related to the GP-3 *post-processing* mode. MATLAB® was used for development, testing and validation. As modified, tested, and validated, the GP-3's *post-processing* mode is now fully operational. The GP-3 is capable of transmitting and receiving bandlimited (3.5 MHz) waveforms at X-Band frequencies. As demonstrated, the GP-3 *post-processing* mode uses MATLAB® to generate and post-process waveforms. System characterization tests included, 1) noise performance, 2) frequency response, and 3) linearity/gain relationships. System noise performance characterization permitted establishment of the receiver 'noise floor' and enabled determination of achievable SNRs (-22 dB to 44 dB for internal noise only). Frequency response characterization provided system 'coloration' effects; an operational center frequency (4.25 MHz) and -3.0 dB bandwidth (4 MHz) were established. The linearity/gain analysis established system input/output power relationships for each channel. The GP-3's operational *post-processing* capabilities were demonstrated for three systems: 1) a digital communication system, 2) a phase-coded, pulse compression radar, and 3) a radar employing nonlinear (range ambiguity) suppression (NLS). As presented, the modifications, validations and documentation provided as part of this research make the GP-3 a viable research testbed – a highly capable system for adding an element of real-world credibility to any experimental, modeling, and simulation scenario.

CHARACTERIZATION AND VALIDATION OF THE GP-3 EXPERIMENTAL RADAR SYSTEM

Chapter 1

Introduction

1.1 Background

The GP-3 is an experimental radar system currently located in AFIT's Department of Electrical Engineering Communications Lab. Originally designed and built for the Air Force Research Laboratory Sensors Directorate RF Sensor Technology Division (AFRL/SNR), it was delivered under contract in a questionable state of operation. In fact, initial problems involving software rendered it useless as a testbed for radar simulations and experiments. Since contractual mechanisms for providing technical support were not in place at the time of system delivery, AFRL sought AFIT's support in characterizing the 'as delivered' performance of the GP-3.

The GP-3 was originally designed to be a general-purpose radar testbed capable of performing virtually any type of radar simulations and experiments within system limitations. Specifically, its stated purpose was "the testing of tactical, airborne, X-Band radar systems, processing techniques and algorithms in a controlled ground-based test range" [1]. However, given the inherent system flexibility built into the system, there are many more potential applications that can be supported. The GP-3 has significant digital signal generation and processing capabilities that are easily controlled through MATLAB® graphical user interfaces (GUIs). When all GP-3 components are fully operational, it provides a versatile testbed for incorporating real-world aspects into both experimental and simulation processes, giving results added validity over computer

simulations. These potential benefits, and the simple fact that the GP-3 has already been designed and built, are key reasons for conducting further research into the design and implementation of both hardware and software components.

The GP-3 consists of two main components including a digital unit and an analog unit. The digital unit is used for all signal generation and processing performed in one of two modes. The *real-time mode* uses a MERCURY® digital signal processing (DSP) board to generate and process transmitted and received signals in real-time. The *post-processing mode* uses MATLAB® to generate and post-process transmitted and received signals. MATLAB® is used for higher-level programming and C is used for specialized routines such as interfacing with the digital-to-analog (DAC) and analog-to-digital (ADC) converters. MATLAB® GUIs and animation facilities are used to interface with the GP-3 and display scenario simulation results [1]. MATLAB® provides a stable environment and allows algorithm and scenario implementations to be programmed relatively quickly. The processing time is acceptable for most scenarios that are within the current performance parameters of the GP-3 [2].

The GP-3 system is designed to transmit and receive up to four separate signals simultaneously. A DAC is used to convert the desired input signal vector (MATLAB® output) to the first intermediate frequency (IF) signal, a 5.0 MHz waveform generated in the digital unit. The resultant IF analog signal is sent to the analog unit, which uses a three-stage up-conversion process to translate the IF signal to X-Band. The system is equipped with pyramidal horn antennas for both transmitting and receiving signals at X-Band. Received signals are down-converted from X-Band to a 5.0 MHz IF and sent

back to the digital unit. After being quantized by the ADC, received signals are processed in either real-time or post-processed depending on the selected operating mode.

Previous GP-3 validation and experimentation has been limited to debugging the delivered MATLAB® GUIs and functions. These efforts resulted in successfully running some system test functions via simulation on separate PCs. These previous efforts identified a number of major software problems severely limiting the GP-3 functionality. The identified software problems included both programming design flaws and problems associated with obsolete software packages. The major software concerns include:

1) Implementation using an obsolete version of MATLAB®,

2) Unorganized file structure,

3) Limited in scope and difficulty in using the delivered MATLAB® GUI,

4) Interfaces between MATLAB® and C and between C and the DAC/ADC are not readily apparent or controllable [2].

The first concern presents a particular problem in that a newer software version may cause existing program codes (e.g., hardware drivers) to 'crash.' The newer version of MATLAB®, version 5.3, does not support all routines of the older version and some programming conflicts exist, e.g., some of the new MATLAB® routines have identical call names as variables used in the original GP-3 code. To ensure the original GP-3 operating structure/system was not destroyed as a result of this research, the original hard drive was mirrored upon delivery to AFIT to ensure delivered system status was recoverable.

The unorganized file structure of the delivered system provided additional concerns. Because of gross inefficiencies in file management, the original hard drive was

cluttered with multiple copies of identical files located in different directories, wasting memory space and making software debugging extremely difficult and even impossible in some cases. The unorganized file structure also made it difficult to determine the interfacing mechanisms between MATLAB® and C. This severely hindered GP-3 use and expansion because new MATLAB® based scenarios were difficult to create. Thus, the delivered system was limited using only the original GUI – a somewhat confusing and difficult implementation that did not run properly upon delivery to AFIT.

As delivered to AFIT, the GP-3 hardware could not be successfully operated; there was insufficient documentation available to accurately characterize software/ hardware interactions and system capabilities as a whole. The GP-3 has potential for becoming an important and valuable research tool, but first, credible documentation must be made available to researchers clearly explaining system capabilities, limitations, and operating procedures.

1.2 Problem

This research focuses on two specific problems that needed addressing before the GP-3 system could be fully utilized. First, the system control software had to be fully understood and debugged and/or rewritten to enhance its functionality. Second, a detailed system evaluation had to be conducted, specifically characterizing GP-3 performance and validating its operation. The results of addressing these issues are then used to make recommendations for further improvements. Software debugging involves mapping and re-organizing the delivered file structure, determining current program implementation of the post-processing mode of operation and rewriting the software to be

more efficient using a robust method. A detailed system evaluation is only possible if all software debugging is accomplished successfully. When complete, software modifications will allow different validation scenarios to be performed, analyzed, and compared to analytic results, making it possible to characterize performance and recommend improvements.

1.3 Scope

This research effort focuses on software modifications and hardware validations related exclusively to the GP-3 post-processing mode. The real-time mode of operation is not addressed because of time constraints and problem complexities associated with it. MATLAB® provides a stable environment for establishing and validating GP-3 performance characteristics, and is used exclusively for development, testing and validation. This thesis effort concludes by demonstrating the post-processing mode is operational by performing a series of different tests, the results of which are analyzed for accuracy.

1.4 Approach

Initially, all effort was directed toward familiarizing researchers with the delivered GP-3 system, including all hardware and software aspects thereof. All available documentation was reviewed and existing MATLAB® and C code was inspected. After safeguarding the original system by mirroring the hard drive, the controlling C code for the channel ADCs and DACs was isolated and targeted as the first area requiring attention – it was important for researchers to establish initial input/output

'communications' with the delivered hardware. The delivered C code structure was used as a basis for rewriting the hardware control code, making the post processing mode operational and allowing the user more control of hardware from MATLAB®. The noise properties (e.g., quantization noise levels, receiver noise floor, filter noise, etc.) and frequency response of the system were then established and characterized using the post-processing mode. Finally, GP-3 operational performance was verified for three distinct systems, including, 1) a binary phase shift keyed (BPSK) digital communication system, 2) a pulsed compression radar using phase coding, and 3) a non-linear, range ambiguity suppression (NLAS) system using interpulse phase coding. In all cases, the generated data was compared to theoretical and analytical predictions.

1.5 Materials and Equipment

This thesis effort was hardware oriented and required the use of the GP-3 Experimental Radar, an oscilloscope, a function generator, and other common laboratory equipment. Sun Microsystems ULTRASPARC® workstations and personal computers were used for post-processing received GP-3 data. MATLAB®, Version 5.3 and Version 4.1c, from The Math Works Inc., Natick, MA, were used exclusively to generate GP-3 input data for all validation and verification testing. All hardware was made available in AFIT's communications/radar laboratory, including the GP-3 Experimental Radar which was on loan from AFRL.

1.6 Thesis Organization

Chapter II gives a detailed description of the entire GP-3 system based on previously published materials and observations made during initial inspections. The research methodology is provided in Chapter III and divided into three phases, including, GP-3 operation, characterization, and validation. Chapter IV provides all the results obtained from characterization and validation testing. The results are used to draw conclusions and form a basis for the recommendations provided in Chapter V.

Chapter 2

GP-3 System Description

2.1 Introduction

The GP-3 system has great potential for performing a myriad of developmental, testing and evaluation operations. This capability stems from the modular system design allowing multiple configurations to be used to accomplish different functions. The following is a detailed description of the digital and analog unit configurations.

2.2 GP-3 Digital Unit

The digital unit contains two 12-bit DAC/ADC boards, a MERCURY® DSP board, a SPARC 10/9U, a 1 GB hard drive, and five expansion ports for additional hard drives and/or CD/floppy disk drives [1]. The SPARC 10/9U, DAC/ADC boards, and MERCURY® DSP board are interconnected through a VME data exchange/control bus. The MERCURY® DSP board description and specifications are not provided here since the real-time operating mode was not within the scope of this research.

2.2.1 Digital Unit CPU

The digital unit CPU is a SPARC 10/9U manufactured by FORCE Computers. The SPARC 10/9U uses a 50.0 MHz processor, 64 MB of DRAM, and supports a 32-bit VMEbus [1]. The current operating system (OS) is Solaris 2.3. In post-processing mode, MATLAB® version 4.1c is used for all high-level programming and C code is used for low-level control such as required for the ADC/DACs. SPARC 10/9U production ended

in 1997 and FORCE Computers only offered CPU hardware support for an additional four years, or until the parts inventory was exhausted.

2.2.2 Digital Unit DACs/ADCs

Interactive Circuits & Systems Ltd. (ICS) makes the ICS-150-ADM boards containing the GP-3's DACs and ADCs. Each board has a total of eight channels, including four DAC and four ADC. However, due to cross-talk interference problems occurring between ADC and DAC channels on a given board, a single board is used for ADC operations and a second board was added for DAC operations [2] – therefore, the GP-3's total capacity includes four DACs (supporting transmit operations) and four ADCs (supporting receive operations). The DAC board has been specifically modified to disable the ADC channels to further reduce potential noise interference. In post-processing mode, the ICS-150-ADM boards are controlled by the SPARC 10 through the VMEbus. The boards have 32-bit front panel ports (FPDPs) which connect to the MERCURY® DSP board for the real-time processing mode implementation.

The ICS-150-ADM board has an internal sample clock and trigger, or, accepts external inputs for the sample clock and trigger. The current configuration has the external clock and trigger inputs from both ADC and DAC boards connected on a separate printed circuit board (PCB), making single external sample clock and trigger inputs. The PCB has a manual switch that toggles between internal and external, both inputs are open-ended TTL connections. Both the ADC and DAC boards can be operated with a 40.0 MHz sample clock for two channels or a 20.0 MHz sample clock for four channels. The internal clocks are programmable in 200.0 Hz steps from 3.75 MHz to

20.0 MHz (40.0 MHz for two channels) [3]. To provide effective sampling rates below 3.75 MHz, a programmable eight-bit decimation control is provided for both the ADC and DAC. The eight-bit decimation provides an effective minimum sampling rate of 3.75/256 MHz = 14.65 kHz. The GP-3 is currently configured with four channels operating at a 20.0 MHz sample clock rate. Changing to two channels requires removing the ICS-150-ADM boards and manually switching to between clock rates. With each change, the controlling C code must be recompiled using parameters matching hardware configuration changes, including sample clock frequencies and internal/external clock and trigger controls.

As configured, the ADC has four operating modes, including 1) continuous, 2) capture, 3) pulse repetition frequency (PRF), and 4) multiple PRF; the mode is set within the controlling C code [3]. The *continuous mode* of operation allows data to be continuously read through any of the destination ports. However, for the VMEbus, an interrupt must be generated for each read out process and each interrupt causes some loss of data, i.e., the readout is not truly a contiguous time sample. Thus, the continuous mode is more appropriately used for real-time processing conditions and was not considered an alternative for post-processing applications of this research.

The GP-3 post-processing mode uses the ADCs configured in the capture mode. The *capture mode* quantizes a fixed number of samples following trigger application. The fixed number of samples is user programmable and can consume all available memory or 128 K samples-per-channel. By default, the GP-3 current configuration automatically sets the number of quantized samples equal to the number of converted DAC samples.

The PRF and multiple PRF modes are in direct reference to radar operations. The *PRF mode* is much like the capture mode in that, following trigger application, a fixed number samples is acquired and output. In this case, the number of programmable samples ranges between 256 and 16384 in steps of 2^n. The *multiple PRF mode* is identical to the PRF mode except it allows multiple captures before data is read from memory. Both the PRF and multiple PRF modes may be combined with either capture or continuous modes of operation. Neither of the PRF modes were used in any scenarios for this research since these modes require a specific sequence of trigger synchronization, an issue discussed later in greater detail.

As configured, the DAC has three operating modes, including 1) continuous, 2) one-shot, and 3) loop. Each mode provides the opportunity for accomplishing different system tests and experiment requirements [3]. The DAC *continuous mode* is very similar to the ADC continuous mode, i.e., the memory buffer is repeatedly reloaded and data is continuously converted to analog. However, as with the ADC continuous mode, this process repeats continuously but does not create a true contiguous waveform. Again, this mode is more effectively used in real-time processing applications and was not considered an alternative for post-processing applications of this research.

The DAC *one-shot mode* corresponds to the ADC capture mode, i.e., a programmable fixed number of samples are converted and the operation is stopped. The number of converted samples is user defined and can be up to 128 K samples. Generally, the GP-3 DACs are configured in one-shot mode for most post-processing applications. However, some system level testing requires the use of the loop mode. The *loop mode* is effectively a continuous one-shot mode, i.e., a single data vector is read into the DAC

memory and repeatedly converted. This mode is ideal for generating periodic waveforms and makes it possible to externally monitor waveforms on measuring devices such as oscilloscopes.

Each of the ADCs/DACs convert using 12 bits-per-sample over a dynamic range of ± 1.024 V [3], corresponding to a quantization step size of 0.5 mV. The maximum number of samples-per-channel, 128 K samples per GP-3 cycle, is equivalent to 6.4 ms of simulation time using a 20.0 MHz sample clock rate. These parameters establish the maximum duration, 6.4 ms, and bandwidth, 10.0 MHz, of data that can be processed over one GP-3 transmit and receive cycle. According to the Nyquist criteria, a 20.0 MHz sample clock rate limits the signal bandwidth to 10.0 MHz. Table 1 summarizes important ADC/DAC specifications that are used in characterizing and testing the GP-3 system.

Table 1. GP-3 DAC/ADC Specification Summary.

Dynamic Range	± 1.024 V
Sample Frequency	20.0 MHz
Bandwidth	0 – 10.0 MHz
Sample Buffer	128 k Samples
Total Time per Buffer	6.4 ms

2.3 GP-3 Analog Unit

The analog unit consists of three separate components contained in one large chassis. The three components include the 1) up-converter, 2) frequency generator, and 3) down-converter. The components reside in the chassis from top-to-bottom as listed. The transmit/receive antennas and necessary interconnecting cables/wires are also associated with the analog unit. Modular in design, the analog unit is versatile and easily upgraded. It has external ports providing X-Band, 30.0 MHz, and 5.0 MHz signal

outputs; this configuration allows for easy addition of external components, interfacing with other RF equipment, and loop-back operations. Having external ports readily available make it possible to take measurements and perform experiments using any of the local oscillator frequencies.

To enable testing as an entire 'system,' the GP-3 is configured for use in simple X-Band indoor test range applications using independent pyramidal horn antennas for each channel or a configuration set up as a four-quadrant receive antenna. The delivered antennas are microwave pyramidal horn antennas with approximate rectangular dimensions of 6.5 x 9.0 cm (11.0 cm diagonally). For almost all scenarios considered for this research, the assumption is made that the receive antenna(s) are in the transmit antennas' far-field region (equivalently stated as plane wave propagation conditions). As defined, an antenna's far-field region is "that region of the field of an antenna where the angular field distribution is essentially independent of the distance from the antenna" [4]. Operating in the far-field region also ensures the receive antennas do not effect transmit antenna radiation patterns (near-field coupling is avoided). The far-field region may be defined analytically as given by (1) where R is the distance from the antenna, D is the largest physical dimension of the antenna, λ is the wavelength defined by (2), C is the speed of light (3×10^8 m/s) and f is frequency [4].

$$R = 2\frac{D^2}{\lambda} \tag{1}$$

$$\lambda = \frac{C}{f} \tag{2}$$

For the GP-3 system, the operating frequency range listed in Table 2 of 9.43 to 9.93 GHz, corresponds to a wavelength, λ, ranging from 3.18 to 3.02 cm. For (1) to be valid, the condition $D > \lambda$ must also be satisfied [4]. For the delivered antennas, the largest antenna dimension, *D*, is the diagonal dimension of 11.0 cm; this satisfies the condition $D > \lambda$ and using (1), the pyramidal horn antennas far-field region is $R > 0.801$ m, or approximately 2'8". Therefore, the transmit and receive antennas should always be separated by a distance greater than 3' to ensure accurate results. Cabling provided with the system allows the transmit and receive antennas to be placed about 10' apart.

Using this modest configuration adds an important element by actually allowing propagation of waves through free-space; this makes it possible to introduce other signals or forms of interference into the system and gives experiments a realistic element that is otherwise not obtainable in computer simulations. When all GP-3 components are fully operational, it provides an extremely versatile testbed – incorporating real-world aspects into both experiment and simulation processes while providing added validity to computer simulation results.

The following is a detailed description of each analog unit component and its function in the transmit and receive processes.

2.3.1 Frequency Generator

The internal frequency generator is not actually in the transmit-receive (Tx/Rx) signal path, rather, it generates the local oscillator (LO) signals required by the up- and down- conversion processes. All GP-3 frequency parameters are listed in Table 2. The internal frequency generator produces a fundamental signal having a frequency of

10.0 MHz. This signal actually 'loops' out of the generator and back into analog unit, allowing it to be removed and replaced with an external signal source. All generated signal frequencies are phase-locked to the fundamental frequency. The X-Band LO frequency is synthesized using a 100.0 MHz source LO. The X-Band LO is tunable from 8.35 GHz to 9.03 GHz in 5.0 MHz increments. The X-Band LO is designated LO1 on the frequency generator rear panel. The tuning process can be controlled locally on the front of the frequency generator or remotely through a serial port. A toggle switch on back of the frequency generator determines the frequency tuning source. The second IF LO is at 870.0 MHz and is designated LO2 on the frequency generator rear panel.

Table 2. GP-3 Frequency Parameters [1].

X-Band Tuning Range	9.43 GHz to 9.93 GHz
X-Band Tuning Steps	5.0 MHz (in 200 *n*Sec)
X-Band Instantaneous Bandwidth	3.5 MHz
X-Band LO (Synthesized)	8.35 GHz to 9.03 GHz
First IF Frequency	900.0 MHz
Second IF LO	870.0 MHz
Second IF Frequency	30.0 MHz
Second IF Bandwidth	3.5 MHz
Third I.F. L.O	25.0 MHz
Third IF Center Frequency	5.0 MHz
Third IF Bandwidth	3.5 MHz
Third IF Stop-Band Frequencies	0 to 10 MHz
Fundamental Source Local Oscillator (LO)	10.0 MHz (All Frequencies Phase-Locked to this Source:Internal or External)
Source LO for X-Band Synthesizer	100.0 MHz
Frequency Stability:	< 10.0 Hz Drift in 0.1 Seconds

The final IF LO, designated LO3, is 25.0 MHz. There are four outputs for each LO but only two are currently used, one for the up-converter and one for the down-converter. The unused LO outputs are terminated with a 50.0 Ω load. The frequency generator has a 20.0 MHz output that can be used as an external clock signal for the DAC/ADCs. The three local oscillators are used to create the IF frequencies in both the up- and down-conversion of signals.

2.3.2 Up-Conversion / Down-Conversion

The up-converter has four input channels and converts the signal from each to an X-Band signal in three sequential operations. The complete analog unit up-conversion process is shown in Figure 1 [5]. The input from the DAC is centered at the 5.0 MHz IF

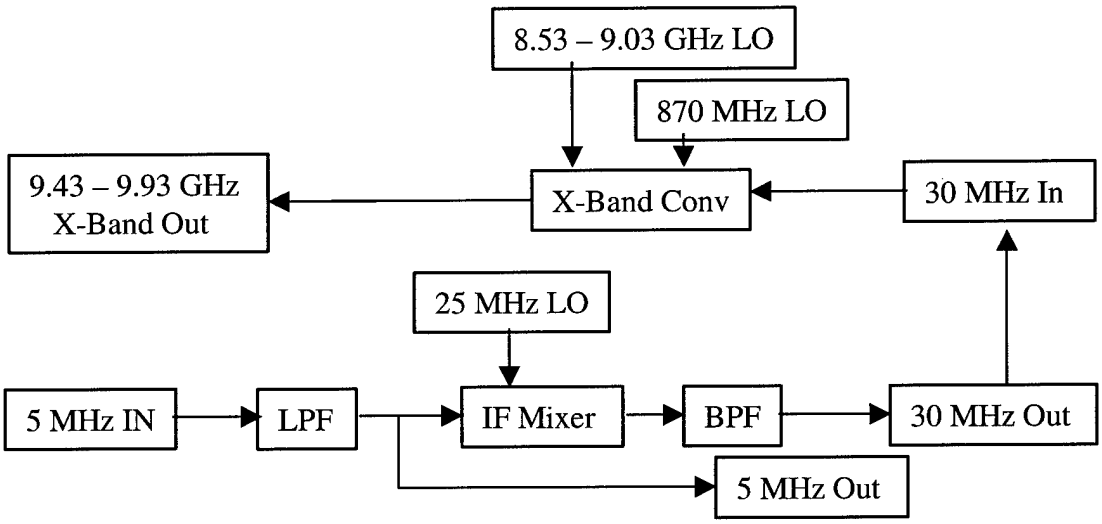

Figure 1. Analog Unit Up-Conversion Process.

with a bandwidth limited by the Nyquist criteria to10.0 MHz. The input signal is lowpass filtered at a bandwidth of 10.0 MHz and power divided with output supplying the up-converter and one supplying the front panel. The up-converted path is mixed with a

25.0 MHz LO, translating the signal to the 30.0 MHz IF. The 30.0 MHz IF signal is bandpass filtered using an effective bandwidth of 3.5 MHz. The 30 MHz IF signal is then mixed with a 870.0 MHz LO creating the first IF centered at 900.0 MHz. This signal is subsequently mixed with the X-Band LO, translating the signal to the desired X-Band frequency location. The X-Band frequency output is adjustable from 9.43 to 9.93 GHz based upon the X-Band LO selected on the frequency generator. The X-Band frequency was 9.43 GHz for all tests and experiments contained in this research.

The analog unit down-conversion process, shown in Figure 2, is nearly identical to the up-conversion except the conversion order is reversed [5]. The fundamental difference is the addition of a low noise amplifier (LNA) to the signal path at the X-Band

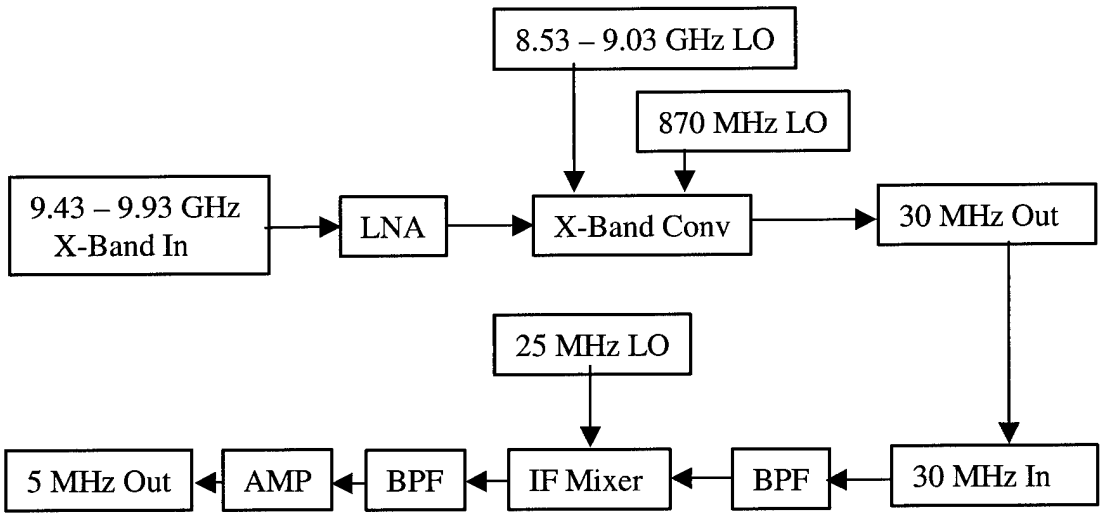

Figure 2. Analog Unit Down-Conversion Process.

input. The LNA amplifies the 3.5 MHz passband signal and attenuates the noise outside the passband, effectively setting the noise floor for the receiver process. The signal is then down-converted through the first, and second IFs to the third IF of 5.0 MHz. The down- conversion process includes a bandpass filter and an amplifier to the signal path.

The bandpass filter has the same 3.5 MHz bandwidth as the other filters used. The gain characteristics of the LNA are neither published nor adjustable. The down-converted signal centered at an IF of 5.0 MHz is output to the ADC, returning the signal to the digital unit.

2.4 System Configuration

The GP-3 post-processing mode uses MATLAB® for generating (transmitting) and post-processing received signals. MATLAB® is used for higher-level programming and C code is used for specialized routines, e.g., interfacing with/controlling the DAC/ADCs. MATLAB® graphical user interfaces (GUIs) are used to interface with the GP-3 and display the simulation results for various scenarios. MATLAB® provides a stable environment where algorithm and scenario implementations can be programmed relatively quickly and easily.

The digital and analog hardware units are only physically connected between the DAC output and up-converter input and between the down-converter output and the ADC input. The DAC and ADC channel designations are identified using notation A1, B1, A2, and B2. The analog unit uses channel designation with the notation CH 1, CH 2, CH 3, and CH 4. It is important to note that for the correct channel designations to match in MATLAB®, the connections between the digital and analog units should be: A1 to CH 1, B1 to CH 3, A2 to CH 2, and B2 to CH 4. The system DOES NOT run in post-processing mode if the compiled C code designators do not match physical hardware settings, specifically, the internal/external clock, trigger setting, and sample clock rate must match identically. When all code parameters match the GP-3 hardware settings the

system is configured for proper operation. Figure 3 represents the complete data/signal processing path of the GP-3 operating in post-processing mode, including the overall transmit and receive processes.

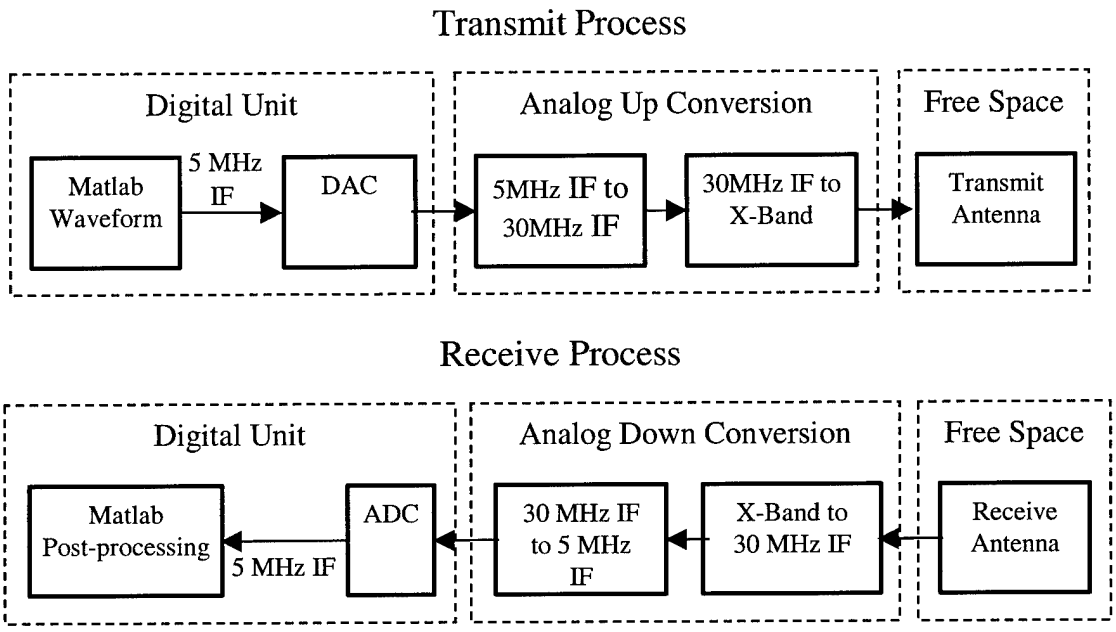

Figure 3. Block Diagram of Transmit and Receive Processes.

2.5 GP-3 Data/Signal Flow

Per Figure 3, digital waveforms are generated in MATLAB® as vectors, where each vector component corresponds to single sample of the desired waveform taken at a sample rate of 20.0 MHz; the input data needs to be equivalent to a generated waveform centered at an IF of 5.0 MHz and having a bandwidth of 10.0 MHz. The digital waveform vectors are passed to the transmit process DAC where the data is converted to an analog signal. The analog signals then pass through the up-conversion, transmission, and down conversion processes of the analog unit before entering the receive ADC at an

IF of 5.0 MHz. After ADC quantization/conversion, the digital data is returned to MATLAB® in vector form and desired post-processing is performed. Not shown in Figure 3, are the connections required to place the GP-3 in 'loop-back' mode, i.e., the transmit X-Band output can be connected directly to the receive X-Band input (bypassing the antennas), or, the transmit 30.0 MHz output can be connected directly to the receive 30.0 MHz input (bypassing the X-Band up/down-conversion), or finally, the transmit DAC output can be directly connected to the receive ADC input (bypassing all analog processing). The basic nature of the post-processing mode allows users almost limitless options for designing and implementing tests and experiments.

Chapter 3

Methodology

3.1 Introduction

This research effort centered on making the GP-3 an operational research tool. The process to make the delivered GP-3 operational progressed through three phases, including GP-3, 1) Operation, 2) Characterization, and 3) Validation. The GP-3 Operation phase includes methods used to get the GP-3 functional, i.e., able to generate/ transmit and receive waveforms using the post-processing mode. Once basic functionality was established, the phase two Characterization process involved various methods for characterizing the GP-3 system. After characterization was complete, to include defining limitations and capabilities of the GP-3, the phase three Validation tasks were undertaken to validate GP-3 system performance for several operational systems

3.2 GP-3 Operation

The first step in the process was to safeguard existing GP-3 software to ensure the status of the delivered system was recoverable. This was done by taking several safety precautions, including, 1) backing-up the original hard drive on tape, 2) putting a second backup copy on the network drive, and 3) duplicating the original hard drive data onto an additional hard drive. The second hard drive became the *experimental drive* allowing software to be edited without risk of losing or damaging the original software configuration.

In an effort to create a more robust system, separate from the existing limited and nonfunctional software, the existing programs were inspected to determine the process

used for controlling and 'communicating' with the DAC/ADC boards via MATLAB®. It was determined that the simplest 'communication' processes were designed for use with some of the original performance tests, such as sending and receiving tones to ensure all channels were functional. As delivered, these tests were designed to use a MATLAB® MEXSOL function compiled using a CMEX compiler, which allows C functions to be called directly from MATLAB®. The MEXSOL function is called *RUNICS* which uses the syntax presented in (3).

$$y = runics(\, x,1\,) \tag{3}$$

When compiled and operating correctly, x is an N-by-4 matrix representing the four channel input waveforms, each N samples long, and y is the N-by-4 matrix created from the quantized received waveforms [2]. Initially, the *RUNICS* function was unable to correctly initialize the GP-3 ADC/DAC boards and caused MATLAB® to crash. After extensive debugging, it was determined that the error was not in the RUNICS function it self, but rather, in the controlling C code for the ADC/DAC boards. The ADC/DAC control file, MAINICS.C, is responsible for initializing and setting all parameters of the ADC/DAC boards. The entire initialization process uses/requires a number of C programs as provided by the ADC/DAC manufacturer, ICS, with the control code calling specific subroutines as needed. Initial debugging involved correcting subroutine call syntax and correctly initializing parameters such that the hardware and software parameters were identical. As a result of these efforts, basic GP-3 functionality was established and transmission/reception of data was possible. However, the original software provided minimal user control of the ADC/DAC via MATLAB® and there were severe trigger problems due to latency.

To provide more user control of ADC/DAC operations from MATLAB®, the MAINICS.C program was revised to include three optional operational modes as selected from MATLAB®. The new operational modes included 1) internal clocking and triggering with ADC capture mode and DAC one-shot mode, 2) external clocking and triggering with ADC capture mode and DAC one-shot mode, and 3) internal clocking and triggering with ADC capture mode and DAC loop mode. The possibility exists to add MATLAB® use control of all parameters, such as clock speed and various combinations of ADC and DAC modes, but was not pursued as part of this research. The options currently supported proved the most useful given an adjustable external clock was not available and the other ADC/DAC modes are not required in post-processing mode. The new options are selected by calling *RUNICS* using the syntax of (4) where *k* is the option selection parameter equal to 1, 2, or 3 corresponding each new operational mode described above.

$$y = runics(x , k) \tag{4}$$

3.2.1 Data Loss Due to Latency

Initial triggering problems caused unacceptable waveform data losses during transmission. The controlling code was written such that the transmitted data was written into DAC memory prior to calling the DAC enabling subroutine. The ADC enable subroutine was then called to begin sampling at the receiver. There was an inherent delay between the actual DAC enable and ADC enable due to software latency that caused the loss of data, i.e, the DAC began to output data before the ADC was enabled. Specifically, the DAC begins to output the converted waveform following application of the first trigger received after DAC enabling; in this case, the trigger comes from an

internal sample clock operating at 20.0 MHz. In terms of actual timing, the first trigger is applied to the DAC before the ADC enable subroutine is completed. The delay is further increased if any internal, higher priority interrupts occur before the ADC is enabled. The resulting data loss averaged approximately 2,500 samples, or 125 μs, and ranged between 1,000 to 50,000 samples with no apparent regularity. Figure 4 shows how the transmitted waveform was received. The transmitted data loss occurs at the beginning of the received waveform, making it almost impossible to determine when the ADC actually began receiving data. Missing the first portion (undetermined amount) of data makes many common post-processing techniques, e.g., correlation, difficult if not impossible to effectively implement. It is possible to avoid the effects of lost data by appropriately delaying the desired transmitted waveform. However, reliably determining a safe amount of delay without significantly reducing the number of useable samples is not necessarily a viable solution to the problem.

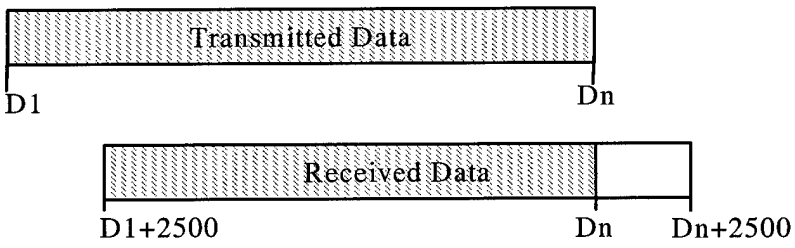

Figure 4. Data Loss Due to Processing Latency.

Further investigation determined that, when using the internal clocking and triggering mechanisms with the post-processing mode, the latency problem is unavoidable. The amount of lost data can be minimized but the effects must still be

considered when using the GP-3 in the post-processing mode. Therefore, an alternate solution was considered.

By rewriting the control code to eliminate different DAC/ADC subroutines such that each is enabled (nearly) simultaneously in the main program, the latency effects were almost completely eliminated (internal interrupt effects were still present but had far less influence on overall latency). The latency effects were further reduced by enabling the ADC before the DAC, thus ensuring the ADC always begins receiving before the DAC output begins. The resulting data loss, now corresponding to data at the end of the transmitted waveform, using the new control subroutine is shown in Figure 5. The average number of lost samples is approximately 750, or 37.5 μs, and ranges from 500 to 850 samples. Although, a clear improvement over the initial data loss figures, this configuration still requires consideration when designing tests and experiments (extra data at the beginning of the received waveform must be ignored and no useful information should be placed near the end of the transmitted data).

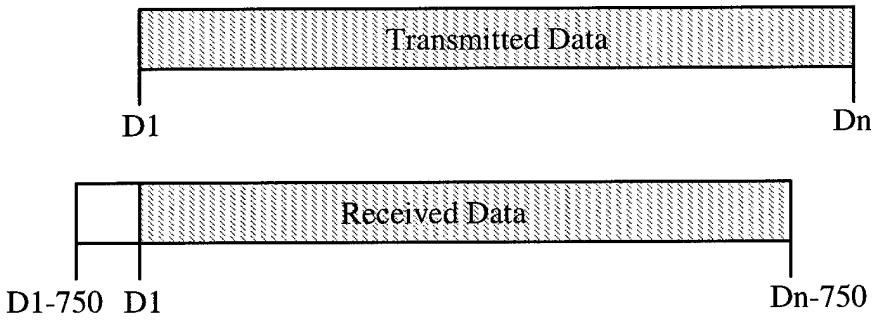

Figure 5. Data Loss Due to Latency After DAC/ADC Software Enabling Improvements.

Data loss due to latency can be avoided completely by using an external triggering mechanism, i.e., an external trigger can be manually applied after both the ADC and DAC have been successfully enabled. The obvious drawback is the external trigger must be applied manually.

Using the external clocking and triggering configuration, the minimum possible delay between waveform transmission and reception was measured. First, the delay was measured through the digital unit by looping straight from the DAC to the ADC, completely bypassing the analog unit. To measure delay, a vector with a one followed by a series of zeros was created in MATLAB® and sent through the DAC to the ADC using the external clock and trigger. The trigger was applied manually after both the ADC and DAC were enabled, eliminating any delay due to latency. The result is shown in Figure 6 where the one occurs at sample number five. Given MATLAB® indexing starts at one, the delay is four samples long which is approximately 200 *n*s for a 20 MHz clock rate. The measured delay results were consistent for all four channels - the delay was never more than five samples (250 *n*s) and never less than three samples (150 *n*s).

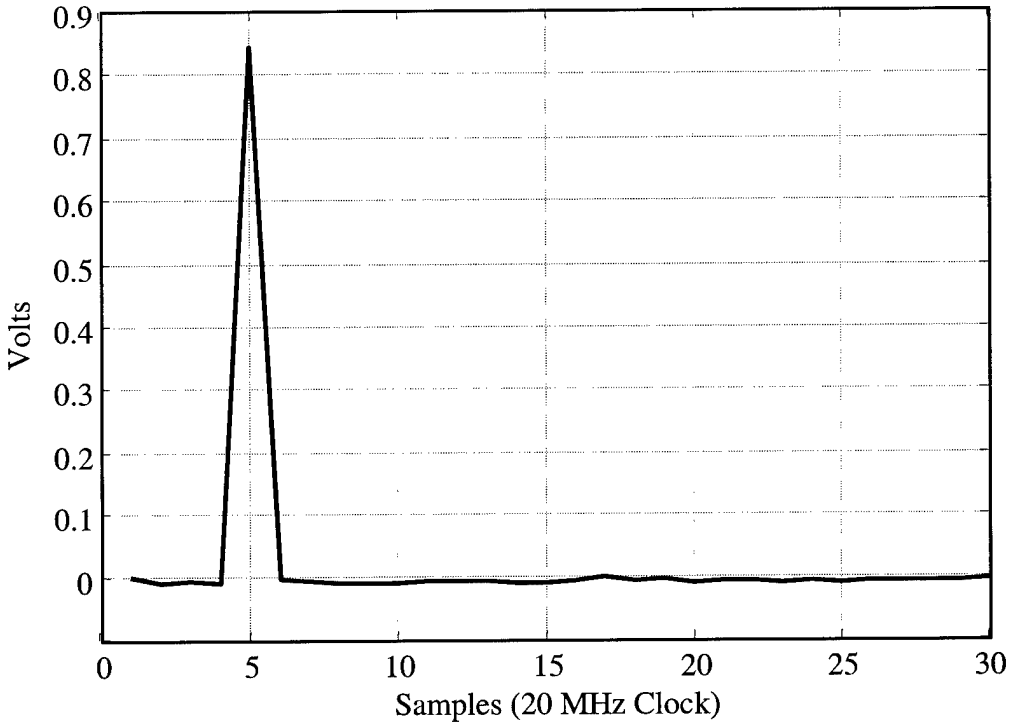

Figure 6. Digital Unit Minimum Delay Estimation.

After determining the minimum DAC/ADC delay, the next step was to determine the minimum delay of the entire system. The same measurement process as before was used except the analog unit was included in the loop (minus the antennas). Figure 7 shows the system delay results for channel 1 where the waveform has propagated through the entire analog unit. The single one followed by a string of zeros is equivalent to inputting a pulse that has infinite frequency content. Given the analog unit has a finite frequency bandwidth, the pulse causes oscillations at a very high frequency. The first effects of the pulse appear near sample number 24, which equates to a system delay of approximately 23 samples (1.15 μs). The results were consistently within ± 1 sample for all four channels tested. The additional delay of 19 samples (950 *n*s), four more than the DAC/ADC results, cannot be totally attributed to path propagation distance since this

would correspond to nearly 285 m – physically impossible given the signal is propagating at the most two to three meters. The inherent delay is actually caused by analog filtering taking place in both the up- and down-conversion processes. The minimum delay between signal transmission and the start of reception is 23 samples, or 1.15 μs.

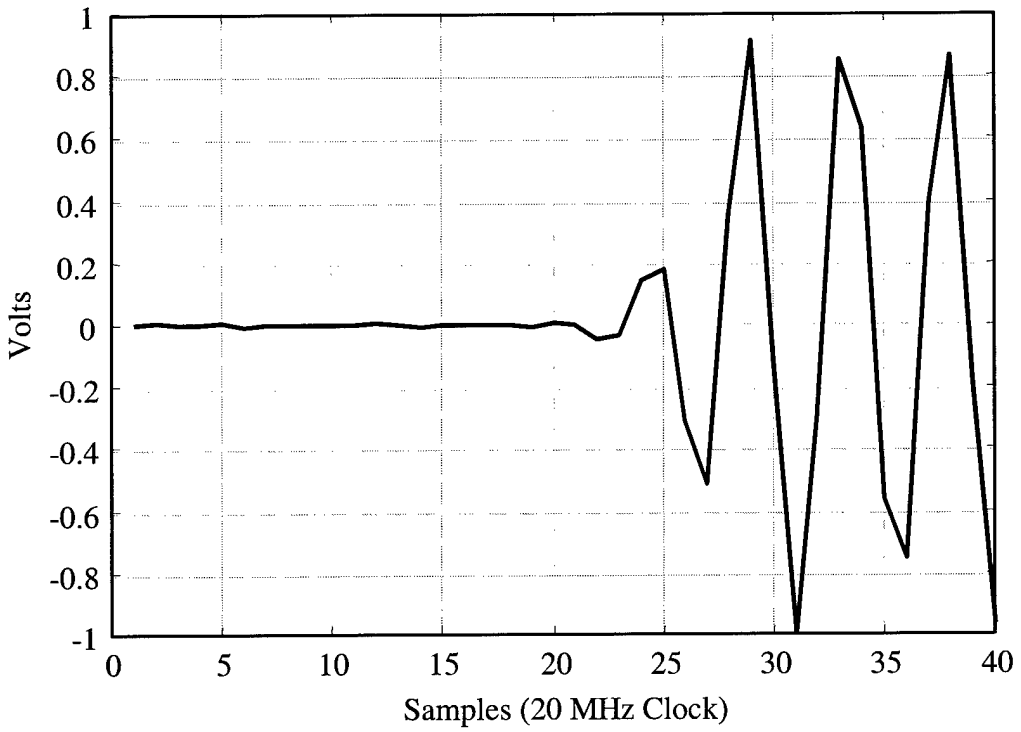

Figure 7. GP-3 System Minimum Delay.

3.2.2 Grounding/Shielding Issues

Another improvement made to the delivered GP-3 system included the addition of a grounding strap between the digital and analog units and improvements to the shielding on some interconnecting cables. Initial GP-3 testing revealed inconsistent noise level and SNR measurement results. After observing drastic noise power variations for separate

transmission scenarios, the analog receiver output was observed on an oscilloscope using the GP-3 loop mode, the mode whereby the GP-3 repeatedly cycles the DAC output and keeps transmitting until interrupted by the user. Inputting a vector of zeros into the DAC is equivalent to turning the transmitter on without transmitting a signal – this scenario allows the total system noise (DAC, transmitter IF/RF, and receiver RF/IF) to be observed on an oscilloscope. By monitoring the noise on the oscilloscope, it was determined that any disturbance of the interconnect cables caused the observed noise amplitude to increase and decrease significantly. When the amplitude increased significantly, it appeared to contain a fundamental sinusoidal component of approximately 5.0 MHz, indicating the interference may be a result of the local oscillator mixing in the IF/RF up (down) conversion processes. The GP-3 local oscillators operate at 8.43 GHz, 870.0 MHz, and 25.0 MHz; the sample rate of both the GP-3 and the oscilloscope is 20.0 MHz. This means any local oscillator interference aliases into the 10.0 MHz bandwidth of the oscilloscope. These results indicated a potential grounding/shielding problem; a grounding strap was connected between the chassis of the Digital and Analog units and the interconnecting cable shields were inspected and reinforced as necessary. Upon completing these operations, the 'Before' and 'After' noise measurement results, illustrated in Figure 8, were obtained and show an approximate 37.0 dB decrease in average noise/interference power.

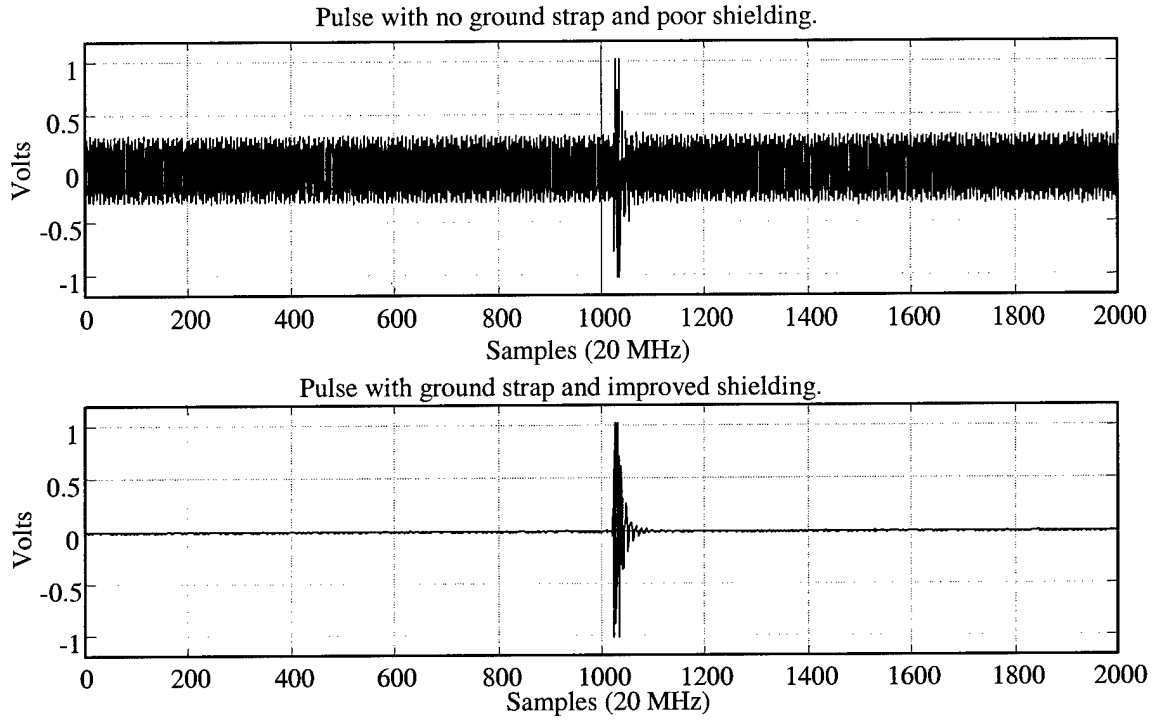

Figure 8. Transmitted Pulse Response Before (Top) and After (Bottom) Adding Ground Strap and Improving Cable Shielding.

3.2.3 ADC Residual Memory

The final improvement made before declaring the GP-3 "fully functional" involved ADC initialization. During simple waveform experiments, i.e., transmitting different waveforms through the DAC/ADC loop, an anomaly was detected. It turns out the ADC 'holds' the last value received from the previous processing cycle until the first value is received from the current DAC transmission cycle. Figure 9 is a plot of the first 2500 samples of the currently received waveform for a transmitted waveform consisting of a string of 128,000 zeros. In this case, the previously transmitted (and received) waveform was a 4.5 MHz square wave containing 128 K samples - the latency delay was 727 samples and the last value received by the ADC was approximately 0.9 V.

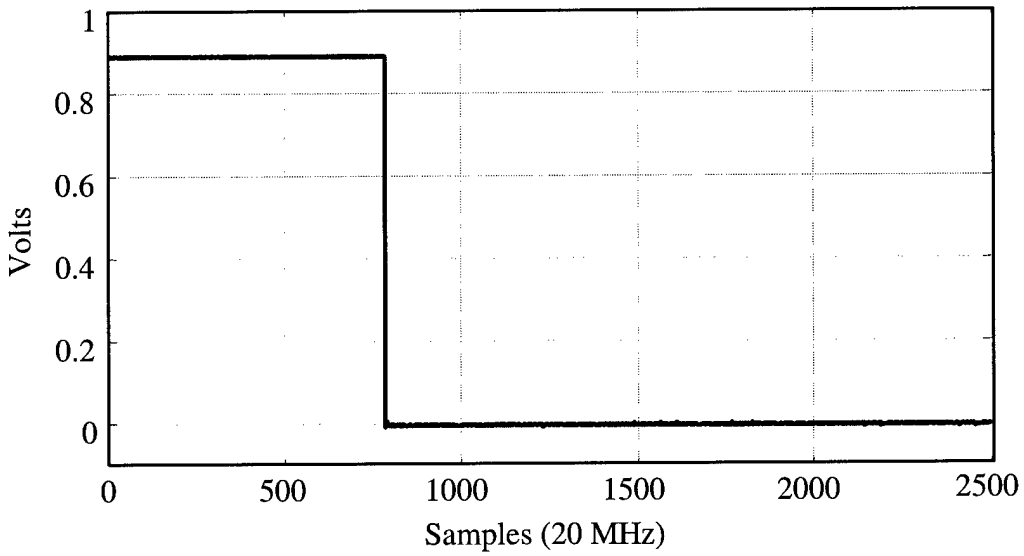

Figure 9. Residual Memory Effects of the ADC.

In Figure 9, the first approximate zero value occurs at sample number 756, approximately 29 samples following the last latent sample. The noted anomaly is a hysteretic effect caused by residual memory within the ADC hardware itself (the on-board DAC/ADC memories are cleared after each processing cycle and thus cannot account for the extra received data at the beginning). Given the ADC turns on before the DAC, there is effectively an "open load" on the ADC input, i.e., a noisy (unknown) input to the ADC which begins quantizing and producing values equivalent to the last value received. Once the DAC turns on and supplies a stable (known) load to the ADC, the ADC begins quantizing to correct values. Although the desired receive waveform is not affected, the results can be confusing and add unnecessary steps to post-processing algorithms.

The hysteretic effects of the ADC were alleviated using an initialization function. An ADC initializing MATLAB® function was written to return the residual ADC memory value to zero. The function, *CLEARICS*, does not contain any parameters or user options, it simply sends a short vector of zeros through the system. This

initialization function is called before *RUNICS* in all GP-3 cycles. Adding the initialization function completed the first phase of the research and the GP-3 was declared "fully functional." The next phase, Characterization, was accomplished to provide researchers an accurate understanding of the GP-3, including limitations and capabilities.

3.3 Characterization

With the GP-3 post-processing mode fully functional, the characterization phase focused on three key areas, 1) system noise, 2) frequency response, and 3) linearity and gain. To be an effective test bed, the GP-3 system noise characteristics had to be fully understood. Knowledge of system noise performance provides researchers with insight into performance limitations in terms of signal-to-noise ratios (SNR). All SNR measurements provided for this research are derived from the quantized received waveform centered at 5.0 MHz IF. The frequency responses provided define the true bandwidths and show how real filter 'coloration' affects signals through each channel. Linearity results are used to establish the relationship between input and output signals and corresponding channel noise powers. It also defines the gain associated with each channel. These are important characteristics that must be made available so appropriate considerations can be made when designing different simulation and testing scenarios.

3.3.1 System Noise

The GP-3 system noise characterization tests were broken down into five categories, including, 1) analog-to-digital converter (ADC) noise, 2) receiver noise floor

(including analog unit), 3) received antenna noise, and 4) system loop noise. The first noise source considered was the quantization noise, i.e., the distortion caused by rounding a continuous analog signal to a discrete quantized value [6]. The GP-3 uses a 12-bit digital-to-analog converter (DAC) in the transmission section and a 12-bit ADC in the receiver section. Quantization noise power resulting from the ADC process may be calculated according to(5), assuming the quantization error is uniformly distributed over a single quantile, where σ^2 is the average quantization noise power and q is the quantile interval, or step size between quantization levels.

$$\sigma^2 = \frac{q^2}{12} \tag{5}$$

In the case of 12-bit conversion, the GP-3 dynamic range is $\pm$ 1.024 V with 4096 total quantization levels, resulting in $q = 0.5\ m$V and $\sigma^2 = 20.83\ n$W per (5).

The first noise characterization tests, referred to as 'ADC Only', included measuring the average ADC output noise power, i.e., measuring the ADC output noise power which includes contributions due to thermal noise, sample clock cross-talk, quantization noise, and other system implementation noises. Noise power measurements were taken by directly terminating the ADC input with a 50.0 Ω load and configuring the GP-3 to receive for the maximum allowable duration of 6.4 *ms* (128K samples for a 20.0 MHz clock rate). The variance of the received noise signal (vector) was then used to estimate the average ADC noise power.

The next noise characterization tests, referred to as 'Receiver Noise Floor', focused on establishing the overall receiver noise floor, accomplished by terminating the receiver X-Band channel inputs and calculating the average noise power in the received signal; these measurements include the cumulative effects of the receiver analog and

digital units, see Figure 3, such as noise due to the low noise amplifiers, IF/RF mixers, bandpass filters, and all other noise associated with the hardware. The average receiver noise power provides an estimate of the receiver system noise floor for each channel.

Noise measurements of received signals collected with the X-Band inputs connected to pyramidal horn antennas, referred to as 'Receive Antennal', provide a measurement of the environment surrounding the GP-3 at the time of the test. These results may change depending on the time of day and look direction of the antenna. In this particular case, the antenna was pointed at a flat cinderblock wall approximately eight feet away and located in room containing numerous personal computers.

The final noise measurements, referred to as 'System Loop', were obtained by connecting the transmitter X-Band outputs directly to the receiver X-Band inputs (eliminating antenna and propagation effects) and transmitting a vector of all zeros (no signal). This measurement includes 'coloration' effects of both transmit and receive processes, i.e., low noise amplifiers, bandpass filters, IF/RF mixers, and thermal noise effects are captured in this measurement.

3.3.2 Frequency Response

In almost all simulations, ideal or flat filter characteristics are assumed. The GP-3 uses real, thus non-ideal, low pass and bandpass filters. The result is system coloration not accounted for by most simulations. To some extent, the exact frequency response of analog filters is unique to each filter. Several methods were considered for obtaining the GP-3 system frequency response. One method, often used for analytic purposes, is to input an impulse and measure the frequency response. At first this seemed a relatively

easy task in the case of the GP-3 radar. However, using a signal vector containing all zeros and a single one (approximately an impulse), provided results that were not measurable and this approach was abandoned.

The second method considered involved measuring the power spectral density (PSD) of multiple tones equally spaced across the bandpass. This would effectively show the frequency response at each tone location with the 'envelope' of all tone responses representing the total frequency response. The accuracy this technique is then dependant on the number of tones used for the measurement. By Fourier transforming the response of each tone, and then squaring the results, an estimate of the output PSD can be obtained which represents the system frequency response. Although not difficult, this process was determined to be too time consuming and was abandoned as well.

The most effective method involved using a PSD estimate obtained from the system response to a swept frequency waveform. A swept frequency waveform was generated using (6), (7), and (8),

$$y(t) = A\cos\left[2\pi\,\theta(t)\right] \tag{6}$$

$$\theta(t) = \left(Bt^2 + Ct\right) \tag{7}$$

$$B = \frac{f_{Final}}{2t_{Final}} \tag{8}$$

where $y(t)$ is the swept frequency waveform, $\theta(t)$ is the time-varying phase responsible for producing the frequency variation, B is a constant based on the desired final frequency, f_{Final}, and the final time, t_{Final}, and C is the desired start frequency.

$$f(t) = \frac{d\,\theta(t)}{dt} = \left(2Bt + C\right) \tag{9}$$

Instantaneous frequency is the time derivative of phase and is calculated according to (9) for the waveform of (7). The envelope and power spectral density (PSD) of the swept waveform are used to display the frequency characteristics or response of each channel.

3.3.3 Linearity and Gain

Characterizing GP-3 linearity and gain involved two separate tests. First, *linearity* refers to how the analog unit affects the amplification/attenuation of signals as they are processed. Ideally, the analog processing of the up-conversion and down-conversion stages, shown in Figure 1, and Figure 2 would only have a linear affect on transmitted and received signals. The frequency response results of the previous section are indicative of the frequency sensitive, non-linearities introduced by the system. Most test scenarios considered for this research required SNRs much lower than the GP-3 is able to produce - given a specific receiver noise floor level, the input signal can only be attenuated so far before it no longer causes any bits to toggle in the DAC of the transmitter. Therefore, noise was added to the system (via directional coupling) using one of the channels as an interference/noise source. This particular linearity test was designed to establish the relationship between average input noise power (transmitter DAC input) and average received noise power (ADC output) for simulated AWGN. The AWGN was created in MATLAB® using the RANDN function as shown in (10) where y is the resultant random noise matrix, P_{IN} is the average input noise power, m is the desired number of rows, and n is the desired number of columns. A linear input-output power relationship makes it possible to design controlled experiments and scenarios with

various SNRs using (11) where P_{OUT} is the desired average output noise power and g is the power gain (absolute) for the channel under consideration.

$$y = P_{IN}^2 \, randn(m,n) \tag{10}$$

$$P_{IN} = \frac{P_{OUT}}{g} \tag{11}$$

The linearity characterization tests were conducted using the entire analog unit in the loop excluding the antennas (the X-Band transmitter output was cabled directly to the receiver X-Band input). The results are used to provide the user with the ability to accurately estimate SNR before performing experiments.

3.4 Validation

The validation phase consists of three potential real-world applications for the GP-3 system, 1) a binary phase shift keyed (BPSK) digital communication system, 2) a pulsed compression radar using phase coding, and 3) a radar non-linear ambiguity suppression (NLAS) system using interpulse phase coding. There are documented theoretical and analytical results for these systems which are compared to measured GP-3 results for validating overall system performance.

3.4.1 BPSK Digital Communication

Theoretical performance of BPSK digital communication systems is well documented. Antipodal BPSK modulation represents the optimum, uncoded binary communication technique [6]. The analytic expression for a BPSK communication symbol is shown in (12).

$$s_i(t) = \sqrt{\frac{2E}{T}} \cos[\omega_0 t + \pi i] \tag{12}$$

The conditions $0 \leq t \leq T$ and $i = 0,1$ apply where T is the symbol duration, E is the symbol energy, ω_0 is the carrier frequency, and i determines the symbol number. The result of (12) is an antipodal signal set containing $s_0(t)$ and $s_1(t)$ which are 180° out of phase and correspond to binary data (bit) values of zero and one. For this research, BPSK communication waveforms were generated in MATLAB® by creating two sinusoidal basis functions 180° out of phase and having duration T. The waveform generation syntax is shown in (13), where A is the amplitude and i equals +1 for a binary '0' and –1 for a binary '1'. These basis functions are then concatenated together in accordance with the order by which the binary data is received – the result is a binary encoded waveform. This process is used to take full advantage of MATLAB®'s matrix manipulation capabilities.

$$basis_i(t) = i A \cos(\omega_0 t) \tag{13}$$

The process for demodulating the BPSK waveform involved using a single correlation receiver. The received signal, $r(t)$, is shown in (14) and consists of a transmitted symbol and $n(t)$, an AWGN process accounting for channel noise effects. The demodulation process involves multiplying the received signal, $r(t)$, by a reference signal, $s_0(t)$ or $s_1(t)$, and then integrating the product over symbol duration T.

$$r(t) = s_i(t) + n(t) \tag{14}$$

$$z_i(T) = a_i(T) + n_0(T) \tag{15}$$

The integration result, $z_i(T)$ shown in (15), will have an integrated signal component, $a_i(T)$, and Gaussian noise component, $n_0(T)$ [6]. The integrated signal component will be

positive or negative depending on 1) the sent symbol and 2) the reference symbol – positive if the two symbols are identical and negative if they are not. This demodulation process is performed in MATLAB® using summation to approximate the integration process (the approximation is good provided sufficient samples are used to represent the waveforms being integrated). In all cases, perfect symbol synchronization is assumed, i.e., the received and reference waveforms align exactly over one symbol interval. This was accomplished in MATLAB® by correlating the entire received signal with the transmitted signal to estimate where symbol boundaries occur. This process is not practical or possible in actual communication systems but is a relatively simple process to use in implementing the GP-3 post-processing mode.

Digital communication system performance is measured and characterized using probability of bit error, P_B, versus E_b/N_0, a dimensionless ratio representing average energy per bit over noise PSD. The theoretical probability of bit error for antipodal BPSK modulation, operating over an AWGN channel, with matched filter detection is given by (16).

$$P_B = Q\left(\sqrt{\frac{2E_b}{N_0}}\right) \tag{16}$$

The Q(•) notation in (16) represents the *complementary error function*, the values of Q(•) are determined from look-up tables [6]. GP-3 system performance for BPSK communications is characterized by comparing measured (simulated) P_B with SNR_{ADC}. In this case, SNR_{ADC} represents the SNR at the receiver ADC output and corresponds to an IF signal centered at 5.0 MHz. To compare GP-3 measured results with established theoretical performance, the relationship between E_b/N_0 and SNR_{ADC} as shown in (17) was

derived [6] where W is the IF bandwidth, S is the average signal power and N is the average noise power.

$$\frac{E_b}{N_0} = TW\left(\frac{S}{N}\right)_{ADC} \quad (dB) \tag{17}$$

In deriving (17), the assumption is made that $N = N_0W$, where IF bandwidth W is usually the signal bandwidth [6]. Using the P_B versus E_b/N_0 performance standard of (16), and the conversion factor provided by (17), results for GP-3 operating as a BPSK digital communication system are compared and its performance validated.

3.4.2 Pulsed Compression Radar

Pulse compression radar waveforms are used to increase unambiguous target range and to improve range-Doppler resolution. Initially, linear frequency modulation (LFM) techniques were used for compression. LFM is still a popular method of pulse compression but there is considerable research being conducted into other pulse compression methods. Maximal length (ML) pseudo-noise (PN) sequences and Gold codes, a subset of ML PN sequences, have inherent qualities that have prompted research into possible pulse compression applications. The research involving GP-3 modeling and simulation focused on using Gold codes for pulse compression [7]. Here, post-processed GP-3 system measurements were used to generate results for comparison with 'real' pulse compression radar data and computer generated analytic predictions.

Pulse compression analytic results are based on the radar ambiguity function as derived from the *time-frequency autocorrelation function* (TEACF). Given complex signal $\bar{s}(t)$, where '$^-$' denotes unit energy, the TFACF is defined as [8], [9], [10],

$$\Phi(\tau, f_D) = \int_{-\infty}^{\infty} \overline{s}(t-\tau)\overline{s}(t)\, e^{j2\pi f_D t}\, dt \tag{18}$$

where τ represents range induced time delay and f_D is the Doppler frequency shift. The *ambiguity function* is simply the magnitude squared of the TFACF. A radar pulse compression signal, comprised of N pulses and P chips, may be expressed as [7]

$$s(t) = \sum_{n=0}^{N-1} \sum_{p=0}^{P-1} u_c(t - nT_r - pT_c)\, e^{j\psi_{np}}\, e^{j2\pi f_0} \tag{19}$$

where T_r is the pulse repetition interval, T_c is the chip duration, ψ_{np} is the phase associated with pulse n and chip p, f_0 is the carrier frequency, and $u_c(t)$ is a rectangular, unit-amplitude pulse of width T_c starting at $t = 0$. Using the pulse compression signal, $s(t)$, and the TFACF, (18), generates an ambiguity surface showing the effects of range delay and Doppler shift. For the $N = 2$ pulse case, Figure 10 shows the ambiguity surface of $s(t)$, including the two range recurrent lobes plus the central primary lobe.

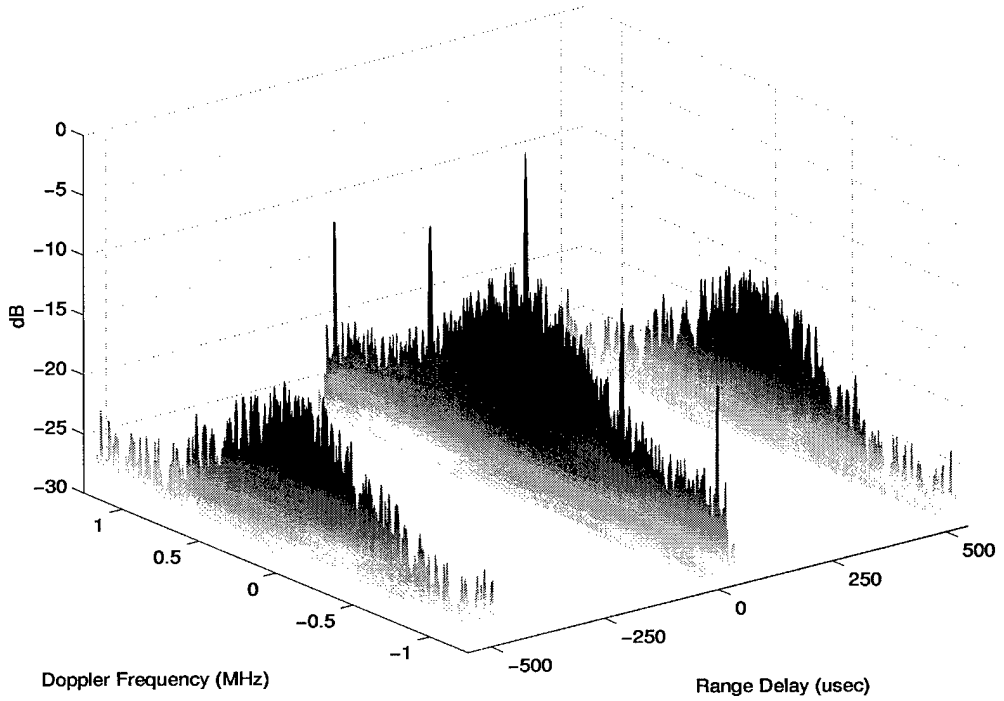

Figure 10. Pulse Compression Ambiguity Surface, N = 2 Pulses, Gold Coded Waveform.

The autocorrelation of the two Gold coded waveforms is essentially a cut of the ambiguity surface at $f_D = 0$, making it a function of τ. Thus, the autocorrelation function gives an indication of the range resolution capability of the coded waveform. The autocorrelation is also equivalent to the matched filter output of a real radar [7]. For this research, post-processed measurements from the GP-3 serve to provide 'real radar' results for transmitted/received Gold coded pulse compression waveforms; results obtained are matched filtered and compared to the analytic autocorrelation function.

3.4.3 Non-linear Range Ambiguity Suppression

Non-linear suppression (NLS) is a novel range ambiguity resolution technique, invented by Carmen Palermo in 1962. Palermo, Leith, and Horgen first reported NLS in

1962, but the available technology at the time prevented further development [11]. A set of M unique pulse codes is selected based on orthogonality criteria or acceptable cross-correlation properties. Each radar pulse is coded with one of M pulse codes and transmitted. After M coded pulses have been transmitted, the process is repeated and another coded pulse train is transmitted. The received target return is simultaneously processed in M independent channels with each channel corresponding to a distinct pulse code. Each channel is designed to suppress returns from all pulses except those containing the code corresponding to that channel. Ambiguity suppression is accomplished through a combination of matched filtering and nonlinear "hole-punching" designed to remove undesired, compressed pulse returns. The channel outputs are subsequently combined, providing the detector with an input signal having ambiguities reduced by a factor of M [12].

To illustrate the concept of nonlinear suppression, the case with $M = 4$ is considered using four distinctly coded pulses, p_1, p_2, p_3, and p_4. The processing flow of a typical NLS receiver channel is shown in Figure 11 and proceeds as follows. First, the complex input data is filtered with h_4, a filter "matched" to coded pulse p_4. The convolution of z[n] with h_4[n] effectively compresses portions of the return containing p_4 pulses while simultaneously "spreading" other data further in time, thus reducing their amplitude.

A nonlinearity ("hole puncher") is next introduced to eliminate the compressed data response. After applying the nonlinearity, the remaining data is filtered using the

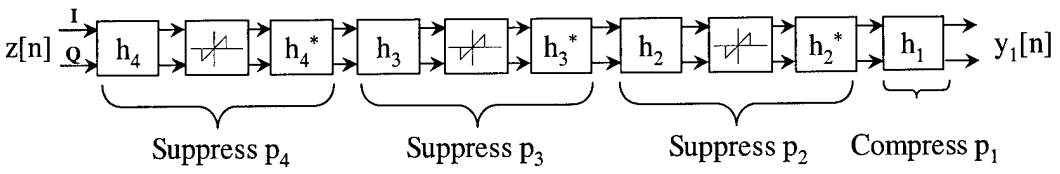

Figure 11. Typical NLS Channel for $M = 4$ Pulse Coding

conjugate of h_4, which is identically p_4, and the original data (minus effects of p_4) is refocused. The compression/puncturing process is sequentially repeated for pulses p_3 and p_2. The final step is to compress the p_1 pulses by filtering with h_1. Ideally, the result is a signal with ambiguities reduced by a factor of four.

Post-processed measurements from the GP-3 are used for a 'proof-of-concept' test to show the improvements indicative to NLS techniques. Figure 12 illustrates the effect of a uniform pulse train operating under range ambiguous conditions where the unambiguous range R_u is dependent upon the pulse repetition interval (PRI) T_r and may be expressed as [12]:

$$R_u = \frac{cT_r}{2} \tag{20}$$

The true range profile of Figure 12 includes three targets at ranges of 0.5 R_u, 2.25 R_u, and 3.75 R_u. Under range ambiguous conditions, the uniform pulse train produces apparent range results at the detector output of 0.5 R_u, 0.25 R_u, and 0.75 R_u, respectively. In this case, the radar receiver is not able to unambiguously resolve the target locations and determine the true range of targets 2 and 3 – under normal operating

conditions the receiver would simply declare three targets present at the apparent ranges and not actually know that an ambiguous condition exists.

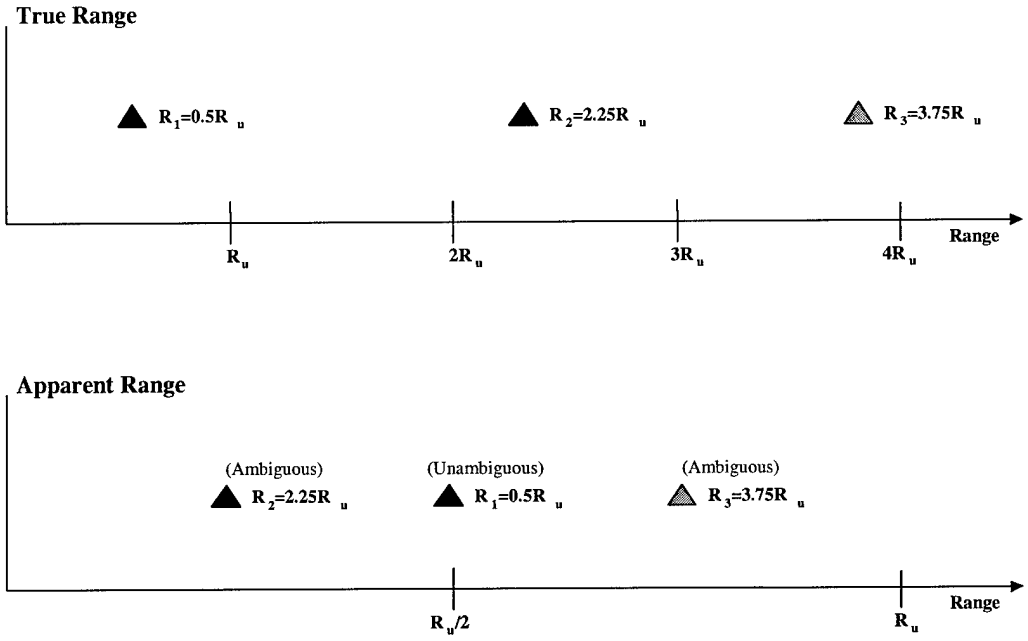

Figure 12. True Range and Apparent Range

The GP-3 is used to simulate radar return data resulting from conditions shown in Figure 12, i.e., the effects of using uncoded, uniform pulse trains under range ambiguous conditions is demonstrated. Results are then generated for the same scenario except NLS processing is employed with four Gold code sequences used as four distinct pulse codes. The results are used to show the added validity the GP-3 system can give to theoretical predictions.

Chapter 4

Results and Analysis

4.1 Introduction

This chapter focuses on providing specific test results obtained for simulations and experiments outlined in Chapter 3. Specifically, system characterization results are presented and analyzed to determine parameters required for the GP-3 validation. Results and analyses of each validation experiment are shown and used to support conclusions drawn about the GP-3 system in Chapter 5.

4.2 Characterization Results

4.2.1 System Noise

GP-3 system noise characterization tests, including, 1) analog-to-digital converter (ADC) noise, 2) receiver noise floor (including analog unit), 3) received antenna noise, and 4) system loop noise, were successful in providing an accurate estimate of system noise performance.

The first noise characterization tests measured the average ADC output noise power. For these measurements, the average of 100 received noise signals was used to estimate the average noise power in each channel. Results of this first series of measurements are shown as 'ADC Only' in Table 3. The 99% confidence interval value is also shown and represents a range about the mean value containing 99% of the data. By comparison with the theoretical ADC quantization noise power, calculated earlier to be $\sigma^2 = 20.83\ n\text{W}$ per (5), the data in Table 3 indicates the average 'ADC Only' noise power is an order-of-magnitude higher for each channel; therefore, system

implementation versus the number of ADC bits drives/establishes the noise performance. These results also show each channel of the ADC has a small DC offset, listed on Table 3 as 'ADC'.

Table 3. Average Normalized Noise Power (Watts).

	Channel 1	Channel 2	Channel 3	Channel 4
ADC Only	4.85 E-7	3.39 E-7	3.03 E-7	8.28 E-7
99% Confidence	± 5.11 E-8	± 2.69 E-8	± 3.84 E-8	± 1.19 E-7
Receiver Noise Floor	6.65 E-7	5.64 E-7	7.08 E-7	1.62 E-6
99% Confidence	± 5.36 E-8	± 3.73 E-8	± 5.27 E-8	± 1.44 E-7
Receive Antenna	6.87 E-7	6.73 E-7	8.65 E-7	1.64 E-6
99% Confidence	± 8.58 E-8	± 3.91 E-8	± 5.52 E-8	± 1.54 E-7
System Loop	1.32 E-5	2.03 E-5	1.03 E-5	1.76 E-5
99% Confidence	± 1.40 E-7	± 7.68 E-8	± 6.72 E-8	± 1.71 E-7
DC Offset / Bias (mVolts)				
ADC	- 8.1	- 4.2	- 4.6	- 2.0
99% Confidence	± 4.35 E-4	± 1.22 E-2	± 4.54 E-3	± 1.27 E-2

The next noise characterization tests focused on establishing the overall receiver noise floor. The average receiver noise power, listed as 'Receiver Noise Floor' in Table 3, provides an estimate of the receiver system noise floor for each channel. The 'Receive Antenna' measurement data in Table 3 represents the average of 10 received signals, instead of 100 received signal used in the other tests. Although not conclusive in and of themselves, the measurements do provide an estimated noise response due to external environmental factors and may be compared with terminated receiver system noise floor levels. In this case, the average noise power increase is not very significant, approximately 0.5 dB across the channels.

The final noise measurement results, listed as 'System Loop' in Table 3, are representative of the noise performance of the entire system. When compared to the

receiver noise floor test results, an estimate of the transmitter induced noise power can be obtained – results indicate an average increase of 12.6 dB in average noise power.

The previous measurements are sufficient to accurately characterize the GP-3 transmitter and receiver processes. Given the dynamic range of the GP-3 is ± 1.024 V with an achievable average signal power of 0.5 W (for sinusoidal signals), and the measured system noise floors are approximately 20.0 μW per channel, the GP-3 can provide signal-to-noise ratios (SNR) up to 44.0 dB. A sinusoid with an amplitude small enough to toggle only one bit in the DAC of the transmitter, ± 500 μV, provides a minimum signal power of 125.0 *n*W. The lowest possible SNR is –22.0 dB (without an external noise source). However, rather than reducing the signal power and utilizing less of the dynamic range available, random noise may be generated and added to ensure the noise has the desired additive white Gaussian noise (AWGN) characteristics.

4.2.2 Frequency Response

The results of using a PSD obtained from the system response to a swept frequency waveform provide an accurate description of the frequency response. The GP-3 uses a 20.0 MHz sample rate, limiting the bandwidth to 10.0 MHz per the Nyquist criteria. The GP-3 analog filters all have a bandpass of 3.5 MHz centered according to the published data provided in Table 2. To completely characterize the frequency response, the swept frequency waveform sweeps from 500 KHz to 10.0 MHz. The frequency resolution, Hz per sample, was approximately 16.0 Hz as established by sweeping 2.0 MHz for each GP-3 cycle of 128 K samples, the total sweep took five GP-3 cycles. The envelope for the total test of Channel 1 is shown in Figure 13, which is a

concatenation of results. The waveform envelope is calculated using the Hilbert transform as shown in (21) where the magnitude of $z(t)$ is the envelope, $y(t)$ is the waveform, and $\hat{y}(t)$ is the Hilbert transform of $y(t)$ [13].

$$|z(t)| = y(t) + j\hat{y}(t) \tag{21}$$

The waveform's amplitude is attenuated according to the filter's instantaneous frequency response. The time domain envelope corresponds directly to the PSD of the swept frequency waveform. The resulting shape is indicative of the frequency response of the system. This result compares very well with MATLAB® generated PSD results. The PSD of Channel 1 is shown in Figure 14.

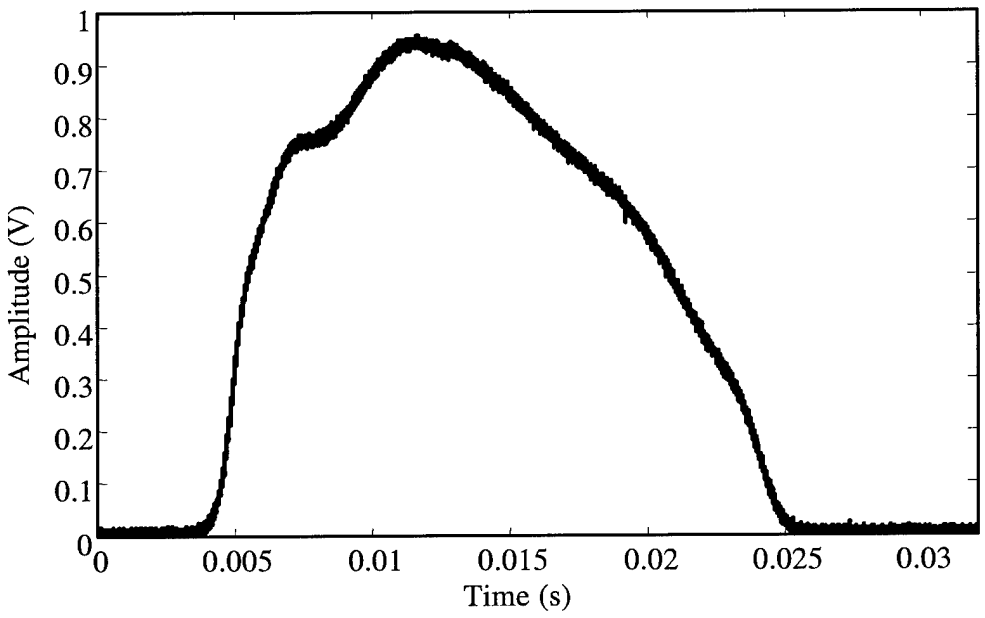

Figure 13. Swept Frequency Waveform Envelope (500 KHz to 10 MHz Sweep).

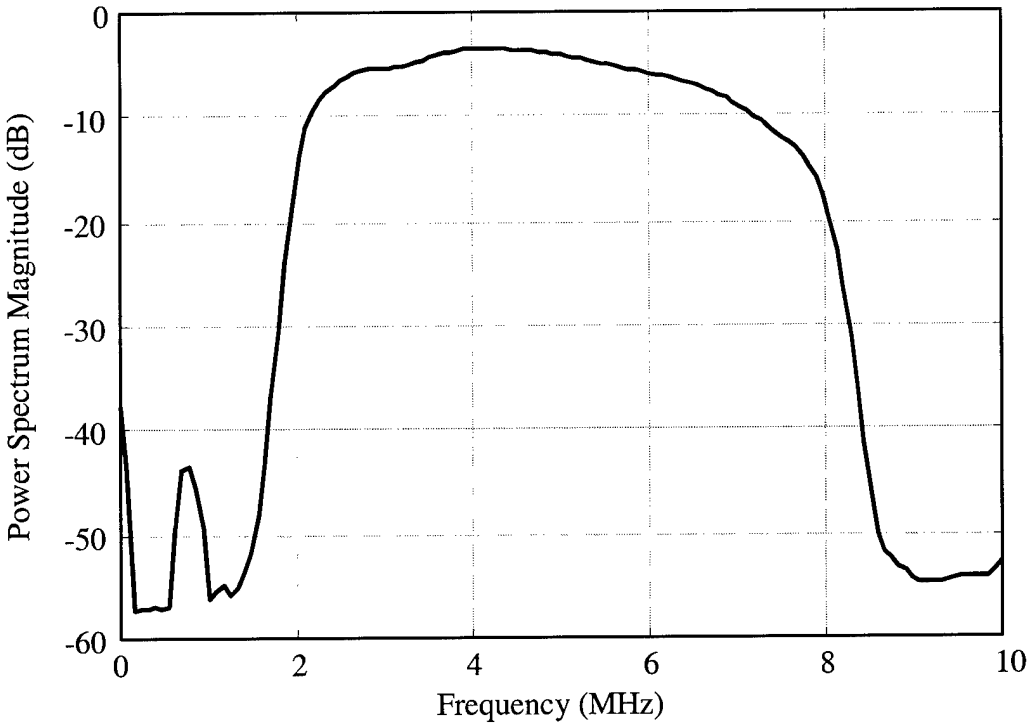

Figure 14. Channel 1 PSD / Frequency Response.

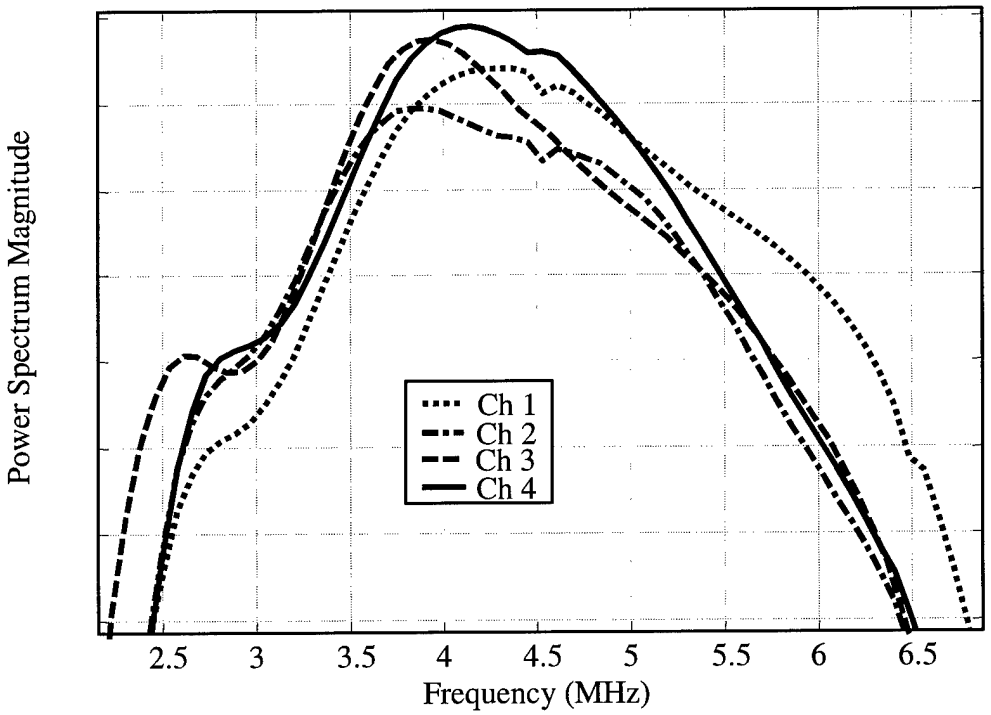

Figure 15. Channel Frequency Responses (-3 dB Bandpass).

The most important frequency response range is the bandpass region. For this research, the *bandpass region* is defined as a frequency band, centered at the frequency response peak, extending to frequency extents where power is attenuated by 3.0 dB. Figure 15 shows the bandpass response/regions for all four channels; clearly, the responses are not flat or ideal in appearance. As indicated, the bandpass region center frequencies are much closer to 4.25 MHz versus the published 5.0 MHz listed in Table 2. The measured –3 dB bandwidth can be generalized for all for channels to 4 MHz. The frequency response curves show the nature of system 'coloration' and indicate the type of effects the system has on transmitted signal amplitude. To utilize the entire dynamic range of the ADC, the input power of the swept tone was adjusted specifically each channel. Thus, Figure 15 DOES NOT indicate the relative gain between channels. The gain associated with each channel is characterized in Section 4.2.3.

4.2.3 Linearity and Gain

The linearity characterization tests were conducted using the entire analog unit in the loop excluding the antennas (the X-Band transmitter output was cabled directly to the receiver X-Band input). Including the antennas in the test would make the test results sensitive to antenna position and surrounding environment. The maximum input noise power was determined for each channel by finding the maximum received noise power such that desired AWGN characteristics were maintained. The maximum input noise power was then decreased incrementally (50 times) to a value of approximately one order-of-magnitude above the system noise floor. The recorded output noise power represents the average noise power for 20 simulations using the same input noise power.

Each noise vector was independently generated using (10) and (11) for values of $m = 1$ and $n = 128$ K , the maximum number of samples available on the GP-3. The linearity test results for Channel 1 are shown in Figure 16 with a linear regression line included for comparison. The correlation coefficient, r^2, was greater than 0.99 for all channels. The gain (g) for Channel 1 was approximately 32.45, or 15.11 dB. The linearity tests results for all four channels are summarized in Table 4.

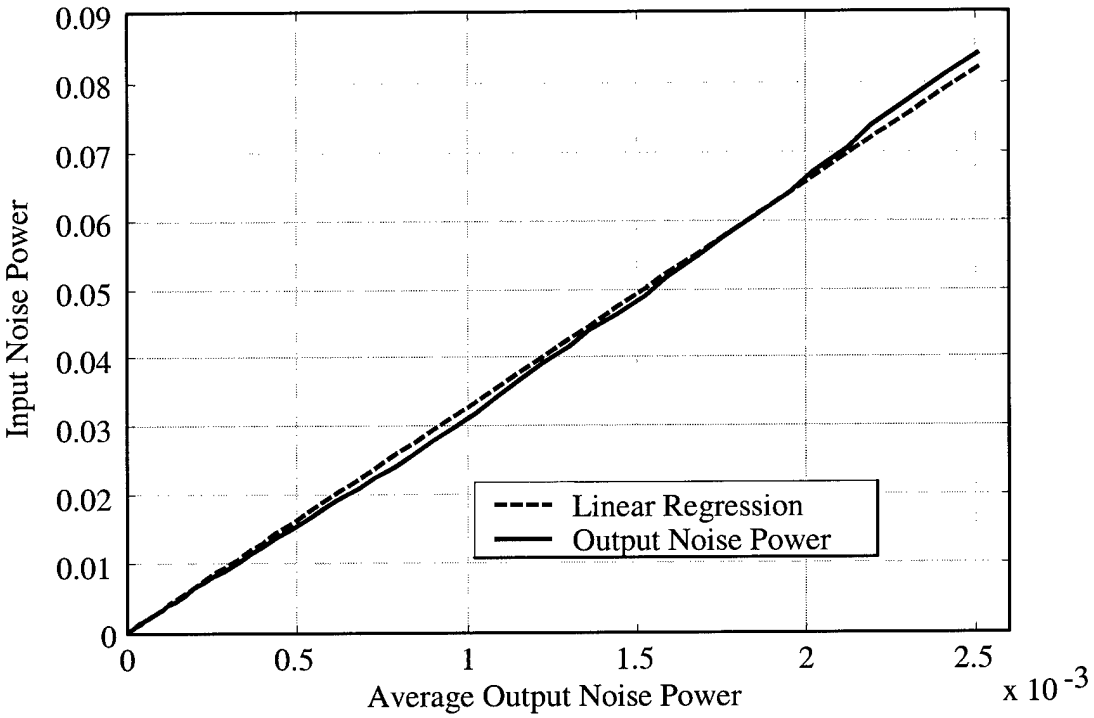

Figure 16. Channel 1 Noise Linearity Characterization.

The same linearity tests were performed using a 4.5 MHz tone to calculate the gain associated with a tone centered within the bandpass region.

Table 4. GP-3 Noise Power and 4.5 MHz Tone Gain (dB)

	Channel 1	Channel 2	Channel 3	Channel 4
Noise Gain (dB)	15.11	16.82	13.18	21.13
99% Confidence	± 0.11	± 0.23	± 0.11	± 0.11
Tone Gain (dB)	18.92	20.32	17.11	23.67
99% Confidence	± 0.11	± 0.20	± 0.07	± 0.14

The GP-3 was configured in the same manner as before, the analog X-Band inputs/outputs were connected directly with no antennas. A sinusoidal tone was generated with a 4.5 MHz center frequency. The tone gain results are included in Table 4 and are clearly higher than the noise gains of the same channel. The difference between the two gains is attributable to the GP-3 filter responses that, as indicated in Figure 15, are somewhat less than ideal. The input noise power spectrum is relative flat before entering the GP-3, i.e., its power is equally distributed across the entire Nyquist spectrum of 0 to 10.0 MHz. However, after passing through the GP-3, the noise spectrum naturally resembles the GP-3 frequency response of Figure 15; the output noise power is distributed according to the filter response over the bandpass region of the GP-3, or approximately 3.5 MHz. This is not the case with the sinusoidal tone since it is initially centered within the GP-3 bandpass region and inherently occupies a very narrow bandwidth relative to the GP-3 filter response – the frequency response 'shape' has minimal impact on 'redistributing' the tone's power.

4.3 System Validation Results

4.3.1 BPSK Communication System

The GP-3 system, when configured to transmit and receive BPSK communication signals, is not simply simulating communication system performance. Rather, it is

capable of representing a complete communication system, including, data generation, signal modulation, transmission, channel effects, reception, signal demodulation, symbol estimation, and bit error calculation. To implement the BPSK communication scenario, two GP-3 transmit channels were used, one for transmitting the BPSK signal and one for transmitting an AWGN signal to represent channel noise effects. The two transmit channel outputs were combined at X-Band using a power divider; thus, the scenario includes all digital (DAC/ADC) and analog (up-/down-conversion) effects with the exception of the antennas. The output of the X-Band power combiner were input to a single receive channel. Based on system characterization results (linearity/filter response), a center modulating frequency of 4.5 MHz was selected. For demonstration purposes, a data rate of 5.0 Kbps was chosen, resulting in only a portion (10.0 KHz) of the total available bandwidth being used. The slower data rate was chosen because of plans to incorporate direct sequence spread spectrum techniques into future scenarios. For the 20 MHz sample rate (consistently used throughout the research), a 5.0 Kbps data rate equates to 4,000 samples per symbol. Given the GP-3 is limited to 128 K total samples per processing cycle/iteration (a function of memory limitations), the maximum number of bits (or equivalently, communication symbols) that can be transmitted/ received per processing cycle is 32. However, due to the latency delay issues discussed in Chapter 3, only 31 symbols are considered per processing cycle. The 4,000 sample 'cushion' created by sending only 31 bits allows the waveform to be padded with 2,000 zeros at both the beginning and end, ensuring all 31 symbols are transmitted and received while completely avoiding data latency issues.

A 31-bit data stream of uniformly distributed bit values was created for each processing cycle by rounding the output of MATLAB®'s *RAND* function to zero or one. For each processing cycle, a different AWGN noise realization was generated using MATLAB®'s *RANDN* function. To remain consistent over the entire scope of GP-3 processing cycles, the signal power remained fixed and the noise power was adjusted to achieve desired SNRs. Initial testing revealed that for 60 processing cycles containing 31 bits (1860 total bits) no symbol/bit errors were detected until SNR = -21 dB, or E_b/N_0 = 7.45 dB per (22). At this SNR level, only two of the 1860 bits were in error which equates to a measured $P_B = 1.075 \times 10^{-3}$. The calculated P_B, using the equivalent E_b/N_0 and Q-function look-up table , is $P_B = 4.0 \times 10^{-4}$ per (16). In this case, the measured P_B is significantly worse than the calculated P_B; clearly, at such low probabilities, 1860 transmitted bits is insufficient to claim statistical significance. However, this did provide a data point for establishing the range of SNR that result in measurable P_B performance.

$$\frac{E_b}{N_0} = TW\frac{S}{N} \tag{22}$$

By incrementally decreasing the SNR and calculating P_B at each SNR, a modest representation of a P_B vs E_b/N_0 curve was obtained following SNR to E_b/N_0 conversion per (22). The resultant curve is compared to the ideal BPSK P_B vs E_b/N_0 curve in Figure 17. In both cases, the curves are relatively flat from –1.5 dB to 2.0 dB because there are no data points over this region. After other measurements had been taken, the P_B measured at E_b/N_0 values of –1.69 dB (–30.14 dB SNR) was taken to establish a lower bound.

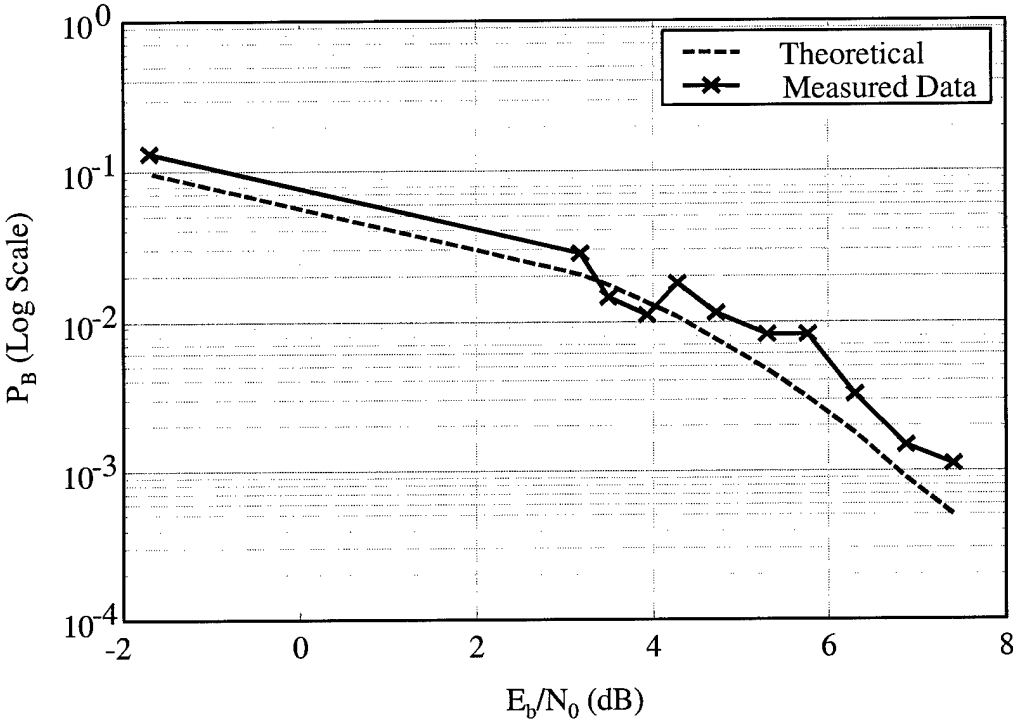

Figure 17. GP-3 Measured BPSK Performance vs. Ideal BPSK.

The limited processing speed of the GP-3 CPU makes complete/statistically significant characterization of the digital BPSK communication system difficult. It takes more than 12 hrs to process 40 processing cycles (12,400 bits). For the –1.69 dB case using 12,400 bits, the calculated P_B was 0.1405 – after using 24,800 bits, the calculated P_B was 0.1320. By comparison, the theoretical P_B is 0.0985. Clearly, as the number of processed bits increased the measured P_B approached the theoretical P_B. The measured curve, while not smooth due to time constraints induced by the limited processing speed, follows the trend of the theoretical P_B. The measured P_B is above the theoretical curve at all but two data points, indicating the assumption introduced earlier that $N_0 = N/W$ is perhaps causing a low estimate of N_0. Thus, there may be more noise power present (at least unaccounted for) in the measured E_b/N_0 used in (22) for converting from SNR. The

results are also expected to vary to some degree, given the 'real system' performance of the GP-3 is being compared to ideal system performance.

4.3.2 Pulsed Compression Radar

Validation with pulsed compression radar performance involves comparing analytic results (calculated using the ambiguity/autocorrelation function) and GP-3 post-processed measurements for a matched filter output using $N = 2$ pulse codes. The two codes used were 31-length Gold codes. The radar parameters included a pulse repetition interval of $T_r = 504$ μsec, a pulse width of $T = 49.6$ μsec containing 31 chips, making chip width $T_c = 1.6$ μsec. Each pulse was modulated using BPSK with a center frequency of $f_c = 5.0$ MHz. As in previous validations, two transmit and one receive channel were utilized for this scenario. The coded pulse waveform was transmitted on one channel and the other channel was used to introduce AWGN into the signal path over free-space. The transmit and receive antennas were set up in a monostatic (co-located) configuration facing a cinder block wall at a distance of approximately eight feet. To prevent possible mutual coupling, the receive antenna was shielded with radar absorbing material. The scenario was repeated twice using an SNR = 28.0 dB, to match analytic results, and an SNR = -15.0 dB, to evaluate waveform response/sensitivity to degraded SNR. The matched filter output for the received waveform was obtained using post-processing; in this case, the post-processing involved carrier removal via mixing and low-pass filtering with a 10^{th}-order Chebyshev filter having a 0.5 dB passband ripple and normalized cut-off frequency of 0.1 (equivalent to 1.0 MHz). The filtering process was followed by

cross-correlation of the down-converted signal with the transmitted signal. Figure 18 shows the post-processed GP-3 matched filter output for the SNR = 28.0 dB case.

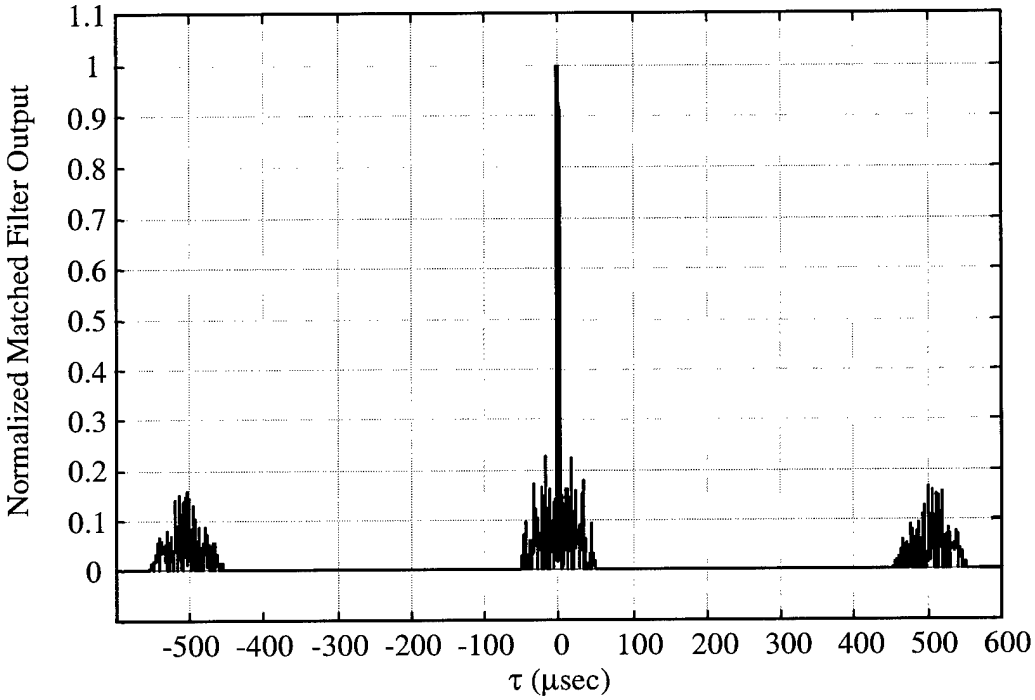

Figure 18. Post-Processed GP-3 Matched Filter Output Results for $N = 2$ Pulses, Gold Coded Waveform at SNR = 28.0 dB.

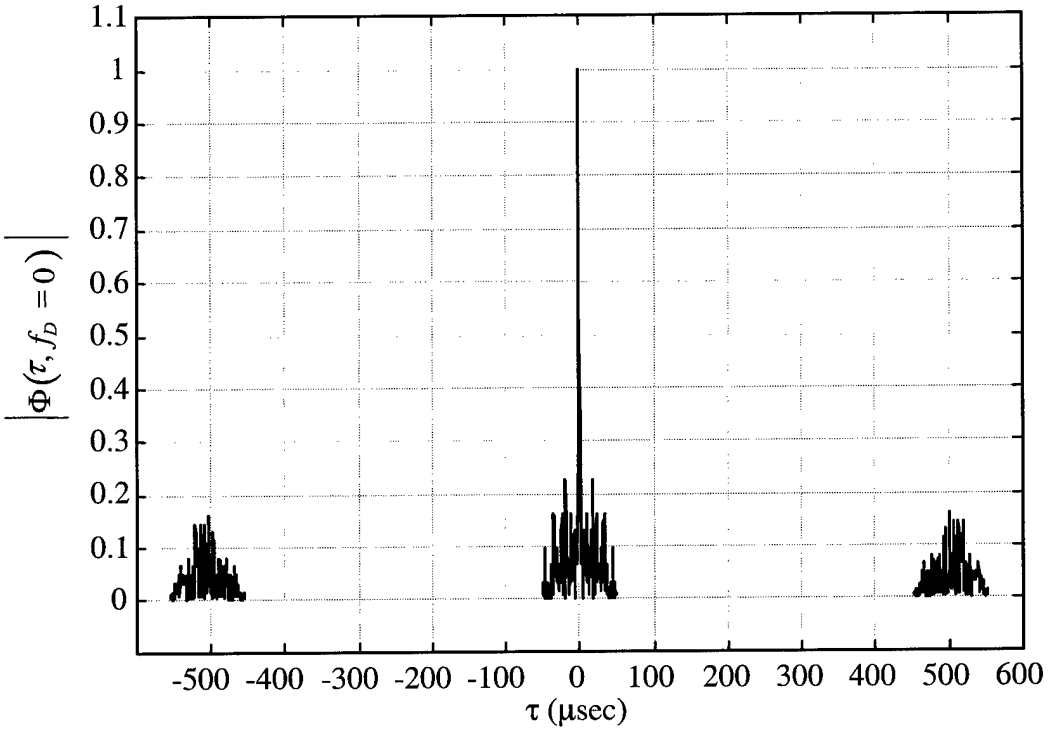

Figure 19. Analytic Autocorrelation Results for $N = 2$ Pulses, Gold Coded Waveform.

Figure 19 is the autocorrelation function for the $N = 2$ pulse case, which is equivalent to the $f_D = 0$ cut of the ambiguity surface shown in Figure 10. With the exception of some small anomalies, the GP-3 measured results in Figure 18 almost perfectly match the analytic results in Figure 19, validating the GP-3 performance. Results of the second lower SNR scenario, shown in Figure 20, are provided to evaluate waveform response due to degrading SNR. These results demonstrate the utility of the GP-3 radar system for conducting parametric sensitivity analyses, i.e., validated system configuration may be extended to include testing conditions which are not always easily modeled.

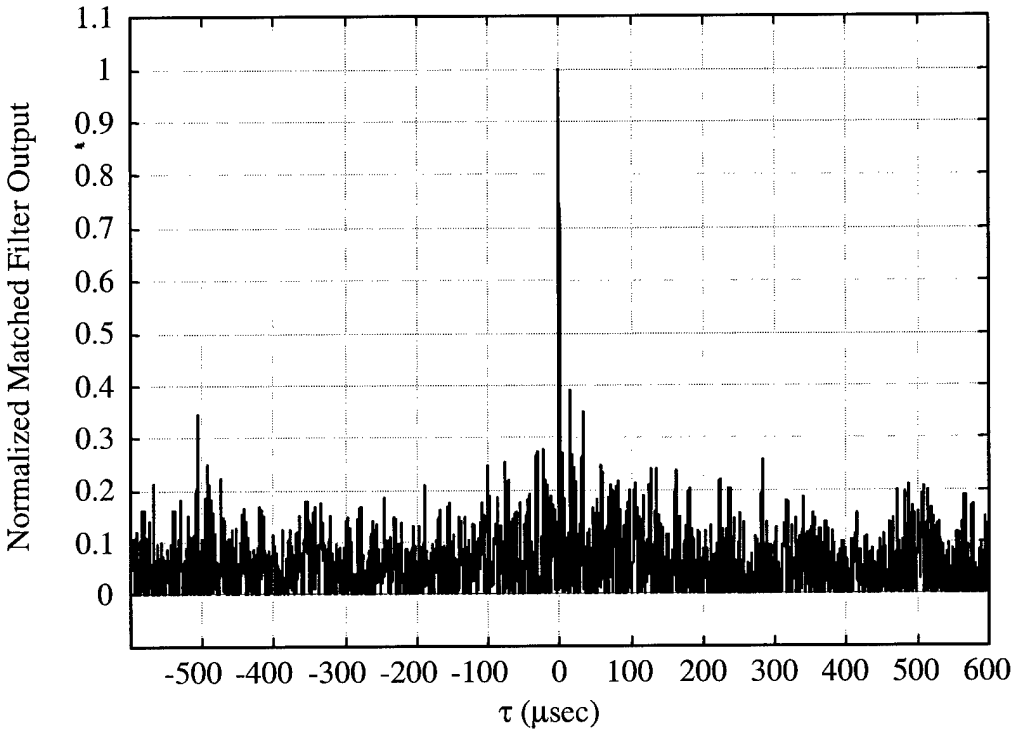

Figure 20. Post-Processed GP-3 Matched Filter Output Results for $N = 2$ Pulses, Gold Coded Waveform at SNR = -15.0 dB.

4.3.3 Non-Linear Range Ambiguity Suppression

This 'proof-of-concept' test was designed using three targets in the configuration depicted in Figure 12. Table 5 lists specific parameters used for NLS testing.

Table 5. NLS Test Parameters.

Parameter	Value
Sample Time (T_s)	0.05 μs
Chip Length (T_c)	0.8 μs
Center Frequency	4.5 MHz
Pulse Length (T_p)	101.6 μs
Pulse Compression Ratio (PCR)	127
Number of Pulse Codes (M)	4
Pulse Coding	Gold Codes
Modulation Scheme	BPSK
Pulse Repetition Interval (PRI)	406.4 μs
Unambiguous Range (R_u)	60.96 km
Target 1 Range	30.48 km (0.5 R_u)
Target 2 Range	137.16 km (2.25 R_u)
Target 3 Range	228.6 km (3.75 R_u)

Due to transmit power and test range implementation issues, it is not possible to actually set up the three targets and take radar measurements. Instead, the ambiguously received target responses were simulated by simultaneously transmitting pulse coded waveforms in the order they would return from each target. Each target return was formatted, delayed, and broadcast over one of three separate GP-3 transmit channels at X-Band. A fourth transmit channel was used to introduce AWGN to the environment at X-Band to produce the desired SNR. The waveforms were transmitted through antennas directed at a cinder block wall approximately eight feet away. The receive antenna was co-located with the four transmit antennas creating a monostatic configuration. Figure 21 shows the order of the transmitted target returns; each target represents a transmit channel. Each of the three target waveforms was delayed by a specific multiple of the PRI, specifically, the Target 1 delay was 0.5 PRI (203.2 μsec), the Target 2 delay was 2.25 PRI (914.4 μsec), and the Target 3 delay was 3.75 PRI (1524 μsec).

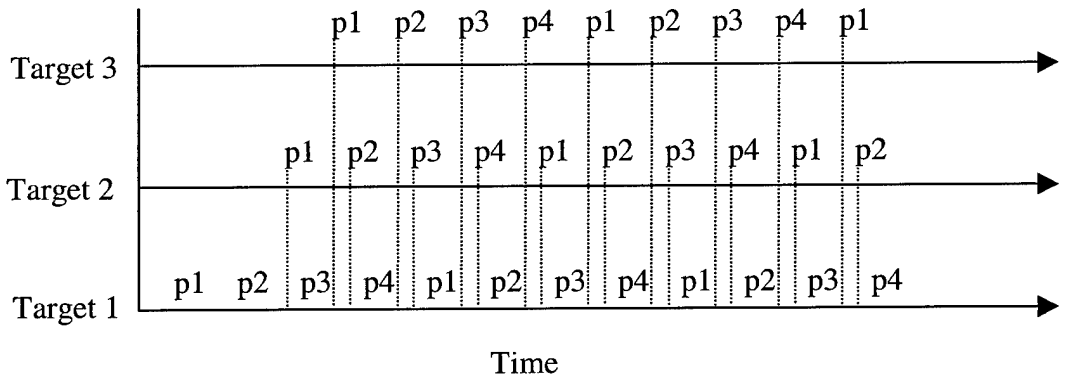

Figure 21. Order of Target Returns for Each GP-3 Channel.

All the waveforms are received through one channel. The dashed lines in Figure 21 provide a picture of the received waveform. For the one pulse code case, p1 was transmitted for every pulse.

The pulse coded waveforms were generated in the GP-3 using the BPSK modulation techniques discussed in the communication system validation section. Four 127-chip Gold code sequences comprised the pulse coding. For this test, all target returns had identical IF SNRs of approximately 10.0 dB

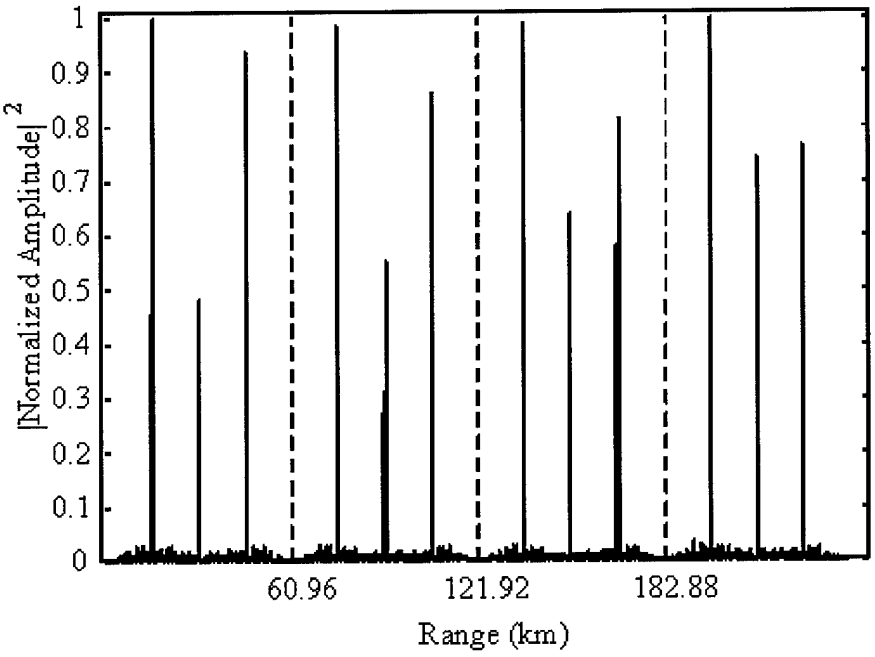

Figure 22. Post-Processed GP-3 Matched Filter Results for NLS Using One Gold Code.

. Figure 22 shows the post-processed GP-3 matched filter results when a single Gold code is used on all pulses – no nonlinear processing is incorporated. The dashed vertical grid lines mark the unambiguous range (R_u) for this particular waveform. As indicated, the ambiguous targets appear exactly as predicted in Figure 12

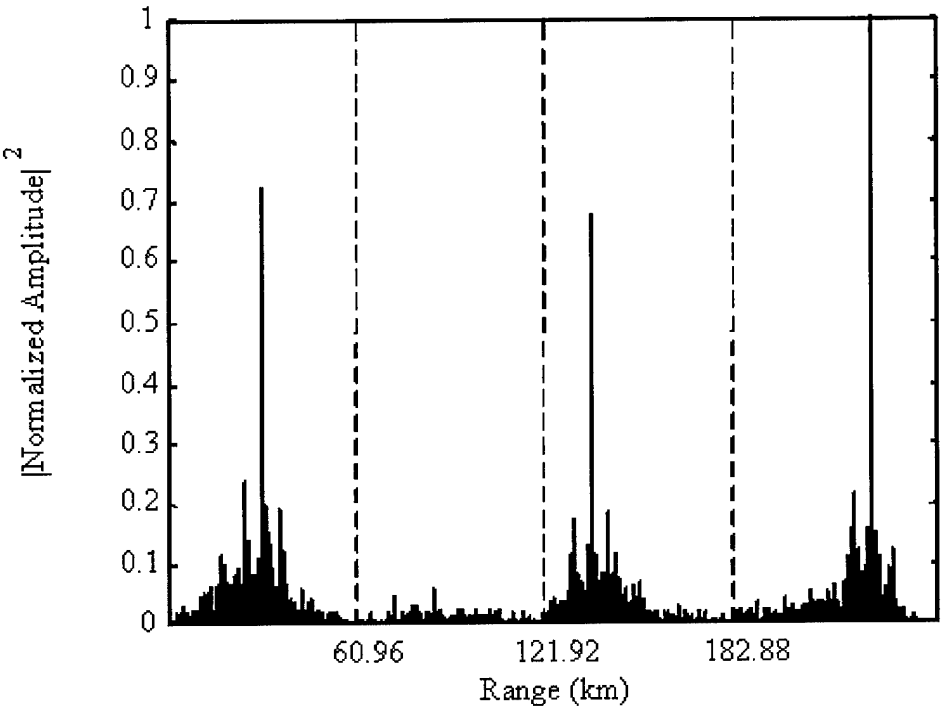

Figure 23. Post-Processed GP-3 Results for NLS Using Four Gold Codes.

Figure 23 shows the post-processed GP-3 results for NLS when using four distinct gold codes – the true target ranges are clearly evident. The higher-level sidelobes appearing in the NLS output are a result of pulse code cross-correlation, autocorrelation sidelobes, and distortion induced by the nonlinearity. Collectively, the results presented in Figure 22 and Figure 23 match predicted NLS results [12], shown in Figure 12, and indicate the GP-3 adds an element of real-world credibility, which is otherwise unobtainable through analytic calculation and computer simulation.

Chapter 5

Conclusions and Recommendations

5.1 Summary

This thesis research focused on characterizing and enhancing the performance of the developmental GP-3 radar system, while placing special emphasis on *post-processing* mode capabilities. An operational *post-processing* mode allows the user to 1) generate specific waveforms, 2) transmit and receive the waveforms, either at IF or at X-Band frequencies, and 3) collect and post-process received waveform data using MATLAB®. The characterization process began with an evaluation of the delivered GP-3 hardware, software, and documentation – without doubt, the delivered system status at best 'questionable' and later determined to be 'inoperable.' The initial evaluation process produced a detailed description of both the digital and analog units. Fundamental system design limitations were identified, including DAC/ADC capability, available memory, processing speed, etc., and were used to form the foundation for conducting a three phase, progressive system characterization to enable the GP-3 to be used as an operational system.

The first phase involved taking steps to enable basic system functionality and consisted of debugging and re-writing control programs to establishing 'communication' between MATLAB® and the DAC/ADC boards. Once basic functionality was established, phase two was undertaken and involved using the GP-3's *post-processing* mode to characterize three main system parameters, including, 1) noise characteristics/ performance, 2) frequency response, and 3) linearity/gain. For phase three, the

characterization results of phase two were used in conjunction with the fundamental limitations identified in phase one to determine possible validation tests for the system. Three validation tests were considered, including, 1) a binary phase shift keyed (BPSK) digital communication system, 2) a pulse compression radar using phase coding, and 3) a radar employing nonlinear suppression (NLS) and interpulse phase coding techniques to reduce range ambiguities. Each validation test fit well within GP-3 operational capabilities and both theoretical and analytic results existed for the scenarios considered – GP-3 measured (post-processed) results could be readily compared as part of the validation process.

5.2 Conclusions

The developmental GP-3 radar system *post-processing* mode has been validated as a viable 'operational' testbed for radar and communications experimentation. The system is capable of generating, transmitting, receiving, and post-processing virtually any analog signal. The effective characterization of system noise performance established the receiver 'noise floor' and made it possible to establish the effective range of possible SNRs as being -22.0 dB to 44.0 dB (without an external noise source). Frequency response characterization results indicate the system 'coloration' caused by filtering and revealed an operational baseband center frequency and bandwidth (- 3.0 dB) of approximately 4.25 MHz and 4 MHz, respectively. The linearity/gain results and analysis establish the relationship between input and output noise powers for each specific channel. This relationship enables the operator to calculate necessary input power to achieve a desired output power. As presented, the modifications, validations

and documentation provided as part of this research make the GP-3 a viable research testbed – a highly capable system for adding an element of real-world credibility to any experimental, modeling, and simulation scenario.

Validation testing of the GP-3's operational, post-processing capabilities was conducted for three specific systems, including, 1) a BPSK digital communication system, 2) a pulse compression radar using phase coding, and 3) a radar employing nonlinear suppression (NLS) and interpulse phase coding techniques to reduce range ambiguities.

For the BPSK digital communication system, the GP-3 system was found to be fully capable of transmitting and receiving digitally modulated signals. The resulting bit error versus average bit energy-to-noise power (P_B vs. E_b/N_0) performance closely matched theoretical P_B vs. E_b/N_0 characteristics – the GP-3 post-processed results were slightly poorer (higher) with the shape of the curve closely following theoretical results. In this case, hardware implementation issues (analog filter responses, non-uniform noise characteristics, etc.) are believed to be responsible for the slightly poorer GP-3 performance.

For validation with the phase coded pulse compression radar, the GP-3 post-processed matched filter results were nearly identical to the analytic autocorrelation function results – the magnitude and relative location of all peaks (mainlobe and sidelobe) were identical. The pulse compression radar tests also demonstrated the usefulness of the GP-3 for furthering research efforts. Once a specific system configuration has been validated, it can be easily modified and used for testing scenarios that are otherwise difficult to model or simulate.

Final GP-3 validation was done using a phase coded radar system with NLS processing to remove range ambiguities. For the multi-target, range ambiguous scenario considered, the multi-channel capability of the GP-3 enabled the system to accurately generate and process a range-ambiguous waveform – the processed waveform reliably mimicked an actual radar return (including point target returns, range dependent signal-to-noise ratios, complex superposition, etc.) and fully demonstrated the potential capability of NLS processing – the degrading effects of ambiguous target returns were nearly eliminated and all three targets were correctly detected at appropriate ranges. Collectively, the GP-3 validation testing provides a basis for characterizing GP-3 operation and declaring it a 'viable' research instrument – this was accomplished using specific system examples to illustrate its usefulness as a reliable testbed.

5.3 Recommendations

Currently, the biggest GP-3 system weakness is the CPU itself. The slow processing speed and outdated software make the entire system incompatible with today's laboratory software and hardware. A CPU upgrade has been scheduled and will certainly enhance the GP-3's current capabilities. This particular upgrade may require a lot of system integration programming if potential compatibility problems come about. The CPU upgrade will present new opportunities for creating robust control GUIs capable of operating with newer versions of MATLAB®. A new CPU also means a newer operating system, allowing the system to be directly accessible over the network and making it possible to access the GP-3 from remote locations.

As currently configured, the external clocks and triggers consists of a single input simultaneously controlling both ADC and DAC; this configuration is certainly impractical from a radar perspective. The ability to apply range gating (selecting data from a particular range cell by turning the receiver on then off for a predetermined interval) is an important function in most radar applications. Thus, modifying the hardware such that a separate trigger is available for the ADC and DAC would provide another important feature to the system.

The existing 12-bit ADC/DAC boards only have enough on-board memory to store 6.4 ms of data for a 20 MHz clock rate; no additional slots or means exists to expand the current memory configuration. This fundamental limitation is perhaps the most limiting feature when using the *post-processing* mode. Newer ADC/DACs with extended memory would greatly enhance system capability and allow longer data collection intervals for post-processing. It should be noted that the current 12-bit output of the ADC/DACs is completely adequate given the current analog hardware configuration; more bits-per-sample are not required given the induced quantization noise is an order-of-magnitude below the established receiver noise floor.

Finally, this research focused exclusively on the GP-3 *post-processing* mode. As delivered, the GP-3 was designed to include a *real-time* processing mode. In this mode, the GP-3 uses a built-in MERCURY® digital signal processing (DSP) board to generate, transmit, receive and process signals in real-time. The *real-time* processing mode needs to be investigated further given its current status is completely unknown. One thing is known for certain, developing the operational *real-time* mode/capability would greatly enhance the potential applications of the GP-3 as a research testbed.

Appendix A

GP-3 Post-processing Operation

A.1 Start-up

Power up Digital Unit (Power switch is on front panel, bottom right corner)

Type "boot disk1" at ok prompt

Login: gp3 (super-user login is "su" or "root" with password "robins")

Password: gp3pass

This will start the OS and bring up a command prompt in the directory "/export/home/gp3".

A.2 Starting MATLAB®

Change the directory to "/export/home/experiment"

Call MATLAB® by typing "matlab"

Setup directory paths by calling "setup"

A.3 Post-Processing Mode Cycle

Generate desired waveforms in MATLAB® for each channel. If a channel will not be used it must still receive a vector. All channels must receive a vector of equal length. Create an Nx4 matrix from the desired waveforms. Transmit and receive waveforms by calling "gp3run". The syntax is shown in (A-1),

$$[y1, y2, y3, y4] = gp3run(x, k) \qquad \text{(A-1)}$$

where x is the Nx4 waveform matrix; k is the mode selector 1, 2, or 3 for 1) internal trigger and clock, 2) external trigger and clock, or 3) DAC Loop mode with internal trigger and clock; y1, y2, y3, and y4 are the received ADC waveforms for each channel with amplitudes scaled to volts. Proceed with any desired post-processing algorithms. All waveform generation and post-processing functions and m-files should be saved in the directory "/export/home/experiment/work".

A.4 Importing Waveforms

Waveforms can be imported from other workstations where newer versions of MATLAB® are available. The waveform '.mat' file must be saved as a version 4 '.mat' file. The import process is performed using the file transfer protocol (FTP). The file should be imported to the GP-3 directory "/export/home/experiment/data". The import process can be performed at any time. After the file transfer has occurred the '.mat' file must be loaded into the MATLAB® workspace. Then the imported waveforms can be transmitted and received using (A-1) providing the waveforms match the syntax explained above. The received ADC waveforms can be saved to a '.mat' file and exported back to the original workstation for post-processing functions using newer versions of MATLAB®.

Appendix B

Programming Code

B.1 ADC/DAC Control C code

This code controls and initializes all the ADC/DAC parameters, when the RUNICS command is executed in MATLAB®.

Mainics.c

```
/* set parameters */

#include "runics.h"
#include "boardlvl.h"

/* -- static variables -- */
static char *Device0 = "/dev/adcf0";
static char *Device1 = "/dev/adcf1";

ICS150_ADCCTRL ctrl1;
ICS150_DACCTRL ctrl2;

void ICSset();

void runics(double *Ypr, double *Xpr, unsigned int len, double
*DacModePtr)
  {
    long    *buf;
    int     DacMode, NumBytes, i;
    double  *Xin;
    DacMode = (int)(*DacModePtr);
    buf = (long *)calloc(len*2, sizeof(long));

    if(buf == NULL)
      { printf("Unable to allocate memory\n"); exit(0); }

    NumBytes      = len * 4 * sizeof(double);
    Xin     = (double *) malloc(NumBytes);

    /* normalized to (abs) <= one */

    NormToOne(Xin, len);

    /* convert to long data and pack data */

    icsPack(Xin, buf, len);

    /* convert to long data and pack data */
```

```
    ICSset(buf, len, DacMode);

    /* convert to double data and unpack data */

    icsUnPack(Ypr, buf, len);

    free(buf);
    free(Xin);
  }

void

/* function ICSset */

ICSset(long *buf, unsigned int len ,int DacMode)
  {
      ID_150  ICS150_0;
      ID_150  ICS150_1;
      ICS150_VMECONFIG VME150_0;
      ICS150_VMECONFIG VME150_1;
      ICS150_ADCCONFIG ADC150;
      ICS150_DACCONFIG DAC150;
      ICS150_FPDPCONFIG FPDP150;
      int     err, i;

      /* Config ICS-150VME ADC*/

      ICS150_1 = ics150open(Device1);
      VME150_1.master = ICS150_MASTER;
      VME150_1.intsrc = ICS150_NONE;
      VME150_1.enableA64 = ICS150_DISABLE;
      VME150_1.A64addr = 0;
      ics150VMEset( &ICS150_1, &VME150_1 );

      /* Config ICS-150VME DAC*/

      ICS150_0 = ics150open(Device0);
      VME150_0.master = ICS150_MASTER;
      VME150_0.intsrc = ICS150_NONE;
      VME150_0.enableA64 = ICS150_DISABLE;
      VME150_0.A64addr = 0;
      ics150VMEset( &ICS150_0, &VME150_0 );

      /* Config ICS-150ADC */

      ADC150.sFreq = 19.99;
      ADC150.chan = 4;
      ADC150.buf = ICS150_SWING;
      ADC150.mode = ICS150_CAPTURE;
      ADC150.prf = 0;
      ADC150.routing = ICS150_VME;
      ADC150.buflen = (long) len - 1;
      ADC150.dec = 0;

      /* Configure ADC Clock and Trigger Source*/

      if(DacMode == 1)
```

```
            {
            ADC150.clksrc = ICS150_INTERNAL;
            ADC150.trig = ICS150_INTERNAL;
            }
           else if(DacMode == 2)
            {
            ADC150.clksrc = ICS150_EXTERNAL;
            ADC150.trig = ICS150_EXTERNAL;
            }

           else if(DacMode == 3)
            {
            ADC150.clksrc = ICS150_INTERNAL;
            ADC150.trig = ICS150_INTERNAL;
            }

      ics150ADCset( &ICS150_0, &ADC150 );

        /* Config ICS-150DAC */

      if(DacMode) {
        DAC150.sFreq = 19.99;
        DAC150.chan = 4;
        DAC150.buf = ICS150_SWING;
        DAC150.routing = ICS150_VME;
        DAC150.buflen = (long) len - 1;
        DAC150.dec = 0;

      /* Configure DAC Mode of operation, Clock and Trigger Source*/
            if(DacMode == 1)
                  {
                  DAC150.mode = ICS150_ONESHOT;
                  DAC150.clksrc = ICS150_INTERNAL;
                  DAC150.trig = ICS150_INTERNAL;
                  }
            else if(DacMode == 2)
                  {
                  DAC150.mode = ICS150_ONESHOT;
                  DAC150.clksrc = ICS150_EXTERNAL;
                  DAC150.trig = ICS150_EXTERNAL;
                  }

            else if(DacMode == 3)
                  {
                  DAC150.mode = ICS150_LOOP;
                  DAC150.clksrc = ICS150_INTERNAL;
                  DAC150.trig = ICS150_INTERNAL;
                  }

        ics150DACset( &ICS150_1, &DAC150 );

        ics150Write( &ICS150_1, buf, 2*len);
      }


/* ADC and DAC Enable routine */
      /* The enable routines are consolidated here to */
```

```
      /* reduce the latency of triggering.  Enabling the */
      /* ADC first ensures the first of the data sent will be */
      /* received. */

ics150ADCCtrlGet(&ICS150_0, &ctrl1);
ics150DACCtrlGet(&ICS150_1, &ctrl2);

ctrl1.enable =1;
ctrl2.enable = 1;

ics150ADCCtrlSet(&ICS150_0, &ctrl1);
ics150DACCtrlSet(&ICS150_1, &ctrl2);


/* END ADC and DAC Enable routine */

      err = ics150WaitADCInt( &ICS150_0, 1000000 );
        if( err != OK )
         { printf("Error: WaitADCInt\n"); exit(0); }


      ics150Read( &ICS150_0, buf, 2*len);


      err = ics150ADCDisable( &ICS150_0 );
      if( err != OK )
      { printf( "Error: ADCDisable\n" ); exit( 0 ); }

/* Wait for key stroke for Loop mode operation */

      if(DacMode == 3)
            {
            printf("Press Any Key to Continue \n");
            getchar();
            }

/* Disable DAC and close ICS boards */

      err = ics150DACDisable( &ICS150_1 );
      if( err != OK )
      { printf( "Error: DACDisable\n" ); exit( 0 ); }


      close( ICS150_0.fd );
      close( ICS150_1.fd );
  }

  /* function ICSset */
```

Bibliography

[1] Y. Salama, D. Miedaner, P. Stockmann, and F. Liu, "GP-3 Band Signal Generation and Processing System," Contract AFRL-SN-WP-TR-1999-1090, Adaptive Technology, Incorporated, 309 Curtis Street, Syracuse, NY 13208, mar 1999..

[2] Culpepper, Edwin. Notes from Presentation and Interview, June 2000. Current Condition and Future Improvements to the GP-3.

[3] Interactive Circuits and Systems Ltd., *ICS-150 Operating Manual.* 5430 Canotek Road, Gloucester, Ontario K1J 9G2, Canada: ICS Ltd, February 1995.

[4] C. A, Balanis, *Antenna Theory Analysis and Design.* 2nd ed. 605 Third Avenue, New York, NY 10158-0012: John Wiley & Sons, Inc., 1982.

[5] ST Microwave Corp., *Analog Hardware Specifications.* 340 N. Roosevelt Avenue, Chandler, Arizona 85226: Signal Technology Corp., 1994.

[6] B. Sklar, *Digital Communications Fundamentals and* Applications. Englewood Cliffs, NJ 07632: Prentice-Hall, Inc., 1988.

[7] T.B. Hale, M.A. Temple, and B.L. Crossley, "Ambiguity Analysis for Pulse Compression Radar Using Gold Code Sequences," *Proceedings of the 2001 IEEE National Radar Conference*, Atlanta, GA, May 2001, pp S3P211-216.

[8] P. M. Woodward, ed., *Probability and Information Theory, With Applications to Radar.* 330 West 42nd Street, New York 36, NY: McGraw-Hill Book Co., Inc., 1953.

[9] C. E. Cook and M. Bernfeld, eds., *Radar Signals, An Introduction to Theory and Application.* Orlando, FL 32887: Academic Press, Inc., 1967.

[10] G. V. Morris, ed., *Airborne Pulsed Doppler Radar.* 685 Canton Street, Norwood, MA 02062: Artech House, Inc., 1988.

[11] Palermo, Leith, and Horgen, *Ambiguity Suppression By Nonlinear Processing*, Eighth annual Radar Symposium Record, June 1962.

[12] J.M. Anderson, M.A. Temple, W.M. Brown, and B.L. Crossley, "A Nonlinear Suppression Technique for Range Ambiguity Resolution in Pulse Doppler Radars," *Proceedings of the 2001 IEEE National Radar Conference*, Atlanta, GA, May 2001, pp S3P271-276.

[13] F. G. Stremler, *Introduction to Communication Systems.* 3rd ed. One Jacob Way Reading, MA 01867: Addison-Wesley Publishing Company, 1990.

[14] S. Oualline, *Practical C Programming*. 3rd ed. 90 Sherman Street, Cambridge, MA 02140: O'Reilly & Associates, Inc., 1997.

Vita

Lieutenant Benjamin Lee Crossley was born in Council, ID. In May 1993 he graduated as valedictorian from Council High School in Council, ID. He received an appointment to and subsequently entered the United States Air Force Academy. After attending two years at the Air Force Academy, he took a two year stop out to serve as a missionary in Japan for the Church of Jesus Christ of Latter Day Saints from July 1995 to July of 1997. Upon returning from Japan, he returned to the Air Force Academy. On June 2, 1999, he was a distinguished graduate, graduating in the top 10% of his class, from the Air Force Academy with a Bachelor of Science in Electrical Engineering. He received his commission on the same day and was selected to attend the Air Force Institute of Technology (AFIT) Master's program at Wright-Patterson AFB, OH. As a Master's candidate in the Department of Electrical and Computer Engineering at AFIT, his focus was on communications and computer networks. He is a member of the engineering society Tau Beta Pi. Upon graduation, he will be assigned to the Air Force Research Labs (AFRL) Sensors Directorate at Hanscom AFB, MA.

Benjamin L. Crossley, Lieutenant, USAF

REPORT DOCUMENTATION PAGE

Form Approved
OMB No. 0704-0188

PLEASE DO NOT RETURN YOUR FORM TO THE ABOVE ADDRESS.

1. REPORT DATE *(DD-MM-YYYY)*	2. REPORT TYPE	3. DATES COVERED *(From - To)*
March 2001	Master's Thesis	

4. TITLE AND SUBTITLE
CHARACTERIZATION AND VALIDATION OF THE GP-3 EXPERIMENTAL RADAR SYSTEM

5a. CONTRACT NUMBER

5b. GRANT NUMBER

5c. PROGRAM ELEMENT NUMBER

6. AUTHOR(S)
Crossley, Benjamin L., Second Lieutenant, USAF

5d. PROJECT NUMBER

5e. TASK NUMBER

5f. WORK UNIT NUMBER

7. PERFORMING ORGANIZATION NAME(S) AND ADDRESS(ES)
Air Force Institute of Technology
Graduate School of Engineering and Management (AFIT/EN)
2950 P Street, Building 640
WPAFB OH 45433-7765

8. PERFORMING ORGANIZATION REPORT NUMBER
AFIT/GE/ENG/01M-06

9. SPONSORING/MONITORING AGENCY NAME(S) AND ADDRESS(ES)
Attn: Edwin B. Culpepper
AFRL/SNRP
WPAFB OH 45433-7765
DSN: 785-4120
edwin.culpepper@wpafb.af.mil

10. SPONSOR/MONITOR'S ACRONYM(S)

11. SPONSOR/MONITOR'S REPORT NUMBER(S)

12. DISTRIBUTION/AVAILABILITY STATEMENT
APPROVED FOR PUBLIC RELEASE; DISTRIBUTION UNLIMITED.

13. SUPPLEMENTARY NOTES
AFIT Technical POC: Michael A. Temple, AFIT/ENG
michael.temple@afit.edu

14. ABSTRACT
The experimental GP-3 radar system was originally designed and built under contract for the Air Force Research Laboratory (AFRL). AFRL sought AFIT's support in characterizing the 'as delivered' performance of the GP-3. This research effort focused exclusively on software modifications and hardware validations related to the GP-3 post-processing mode. As modified, tested, and validated, the GP-3's post-processing mode is now fully operational. The GP-3 is capable of transmitting and receiving bandlimited (3.5 MHz) waveforms at X-Band frequencies. System characterization tests included, noise performance and frequency response. System noise performance characterization permitted establishment of the receiver 'noise floor' and enabled determination of achievable SNRs (-22 dB to 44 dB for internal noise only). Frequency response characterization provided system 'coloration' effects; an operational center frequency (4.25 MHz) and -3.0 dB bandwidth (4 MHz) were established. The GP-3's operational post-processing capabilities were demonstrated for three systems: 1) a digital communication system, 2) a phase-coded, pulse compression radar, and 3) a radar employing nonlinear (range ambiguity) suppression (NLS). The GP-3 is now a viable research testbed - a highly capable system for adding an element of real-world credibility to any experimental, modeling, and simulation

15. SUBJECT TERMS
GP-3, Experimental Radar, Research Testbed, Non-linear Suppression, Pulse Compression Radar, BPSK communication , Signal Post Processing

16. SECURITY CLASSIFICATION OF:			17. LIMITATION OF ABSTRACT	18. NUMBER OF PAGES	19a. NAME OF RESPONSIBLE PERSON
a. REPORT	b. ABSTRACT	c. THIS PAGE			Dr. Michael A. Temple, AFIT/ENG
U	U	U	UU	90	19b. TELEPHONE NUMBER *(Include area code)* (937) 255-3636, ext 4703